

## HIV infection is influenced by dynamin at three independent points in the viral life cycle

Anupriya Aggarwal<sup>1</sup>, Tina L. Hitchen<sup>1</sup>, Lars Ootes<sup>1</sup>, Samantha McAllery<sup>1</sup>, Andrew Wong<sup>1</sup>, Khanh Nguyen<sup>1</sup>, Adam McCluskey<sup>2</sup>, Phillip J. Robinson<sup>3</sup> & Stuart G. Turville<sup>1</sup>

<sup>1</sup>The Kirby Institute, University of New South Wales, New South Wales, Australia.

<sup>2</sup>Centre for Chemical Biology, Chemistry, School of Environmental and Life Sciences, The University of Newcastle, Callaghan, Australia

<sup>3</sup>Children's Medical Research Institute, The University of Sydney, New South Wales Australia

### *Corresponding Author:*

Stuart G. Turville

The Kirby Institute, UNSW Australia

Office 529 Level 5 Wallace Wurth Building,

UNSW, Sydney NSW 2052

Telephone: +61 (02) 9385 0462

Email: sturville@kirby.unsw.edu.au

**Running title:** *HIV infection is dynamin dependent and not related to HIV endocytosis*

### **Abstract**

CD4 T cells are important cellular targets for HIV-1, yet the primary site of HIV fusion remains unresolved. Candidate fusion sites are either the plasma membrane or from within endosomes. One area of investigation compounding the controversy of this field, is the role of the protein dynamin in the HIV life cycle. To understand the role of dynamin in primary CD4 T cells we combined dynamin inhibition with a series of complementary assays based on single particle tracking, HIV fusion, detection of HIV DNA products and active viral transcription. We identify three levels of dynamin influence on the HIV life cycle. Firstly, dynamin influences productive infection by preventing cell cycle progression. Secondly, dynamin influences endocytosis rates and increases the probability of endosomal fusion. Finally, we provide evidence in resting CD4 T cells that dynamin directly regulates the HIV fusion reaction at the plasma membrane. We confirm this latter observation using two divergent dynamin modulating compounds, one that enhances dynamin conformations associated with dynamin ring formation (ryngo-1-23) and the other that preferentially targets dynamin conformations that appear in helices (dyngo-4a). This in-depth understanding of dynamin's roles in HIV infection clarifies recent controversies and furthermore provides evidence for dynamin regulation specifically in the HIV fusion reaction.

This article has been accepted for publication and undergone full peer review but has not been through the copyediting, typesetting, pagination and proofreading process, which may lead to differences between this version and the Version of Record. Please cite this article as doi: 10.1111/tra.12481

## Introduction

The enveloped human immunodeficiency virus type 1 (HIV-1) is a retrovirus capable of penetrating its target cells by fusion of its viral membrane with membranes in the targeted cell<sup>1</sup>. Cellular entry by fusion is preceded by a set of well-characterised interactions involving glycoproteins in the viral envelope, the CD4 receptor and one of the coreceptors CXCR4 or CCR5<sup>2-7</sup>. The mechanism of interaction of HIV with these receptors is well characterised and leads to specificity of cellular recognition, altered protein conformation, membrane fusion and productive entry to the cell cytoplasm<sup>8</sup>. While the mechanism of fusion is well understood, the specific site of fusion remains controversial. There are two primary entry sites: directly from the plasma membrane or from membranes of the endolysosomal system following endocytic uptake of the virus<sup>9-30</sup>. Alternative entry sites have been explored in a wide range of cell types and one common theme is that productive infection requires the GTPase enzyme dynamin<sup>18,21,24</sup>. These studies do not explain how or whether dynamin might play a role at both fusion sites or at additional stages of the virus life cycle.

The majority of observations supporting HIV fusion being dependent on endocytosis have been made largely in HeLa cells. In this cell type evidence is drawn from live single particle viral tracking, the emergence of new generations of potent endocytosis inhibitors targeting either dynamin (herein with will refer to dynamin I and dynamin II jointly, since current generation dynamin inhibitors do not discriminate) or clathrin<sup>21,24,31</sup> and the use of cell impermeable inhibitors (HIV fusion inhibitors T-20 and C52L).

In CD4 T cells the fusion mechanism is presently controversial, with evidence for or against HIV fusion from within endosomes. For instance, T cell lines can be engineered to express a dominant negative version of dynamin, in turn lacking constitutive endocytosis and yet are still permissive to HIV fusion<sup>25</sup>. In contrast, small molecule dynamin-targeted inhibitors can block both endocytosis and HIV fusion in primary activated CD4 T cells<sup>24</sup>. Assays that incorporate cell impermeable fusion peptides in cell lines and activated CD4 T cells also show mixed results, with surface accessibility of the HIV fusion reaction (plasma membrane fusion) supported in one study<sup>25</sup> and not supported by others<sup>21,24</sup>. Whilst resting CD4 T cells can also play an important role in HIV persistence<sup>32</sup>, there are no observations at present that define the HIV fusion site in this important HIV target.

One hypothesis emerging from the present controversy of the HIV fusion site, is the regulation of HIV infection by dynamin independent of its role in HIV endocytosis. Alternative and/or additional roles for dynamin in the HIV life cycle are supported by dynamin's multifaceted role in the cell which includes: endocytosis at the plasma membrane<sup>33</sup>, F-actin regulation<sup>34-36</sup> and cytokinesis at the mid-body during mitosis<sup>37,38</sup>. Each of these roles has the potential to influence HIV infection through initial endocytosis of the HIV particle<sup>21</sup>, dynamics and influence of F-actin at the cortex<sup>39-44</sup> and regulation of HIV infection through cell cycle progression<sup>45</sup>.

To help resolve inconsistencies with regard to the HIV fusion site in primary CD4 T cells and to further test the hypothesis that HIV entry is dependent on viral particle endocytosis, our broad aim is to gain a mechanistic understanding into how dynamin inhibition influences various stages of the HIV life cycle. The primary focus of our study revolves around two major *in vivo* HIV targets: Resting and activated CD4 T cells. As HeLa cell lines have been primarily used in the study of dynamin's influence, we have systematically incorporated them alongside primary T cells.

## Results

### *Endocytosis inhibitors block HIV at multiple time points*

Our initial aim was to determine the timing of action of dynamin inhibitors during the HIV life cycle. In the time of addition assay the temporal effect of dynamin inhibitors is compared to the effects of well-characterised HIV antiretrovirals on entry, reverse transcription and integration. The time taken for HIV to become refractory to the HIV antivirals serves as time stamp marking completion of that viral event and in turn defines the kinetics of each discrete step in the virus life cycle: (Fig 1A). For dynamin inhibition time-of-drug-addition experiments, the small molecule inhibitor dyngo<sup>®</sup>-4a was used since: i) it has specific activity towards the dynamin helices that are required for endosomal scission<sup>46</sup>; ii) it was significantly more potent in HIV inhibition than dynasore in initial HeLa cell infections (data not shown). The small molecule clathrin inhibitor pitstop<sup>®</sup>-2 was also as a control condition to block endocytosis via a different mechanism to dynamin. Together they allow a discrimination of endocytosis from other dynamin functions that are known to not involve clathrin<sup>31</sup>. We initially tested dynamin inhibition in HeLa cell lines engineered to detect HIV infection (TZM-bl) to reproduce published data and then subsequently compared the observations to those in primary CD4 T cells.

Consistent with previous reports<sup>21,24</sup>, dyngo-4a and pitstop-2 equally inhibited HIV infection in HeLa cells (Fig. 1). Fortunately, in HeLa cells we could equally test the inhibition in CCR5 using HIV strains (HIV<sub>Bal</sub>) in addition to CXCR-4 using HIV (HIV<sub>NL43</sub>) (data presented hereon in HeLa cells is representative of both HIV<sub>Bal</sub> and HIV<sub>NL43</sub> infections). Using the HeLa cell model, we then mapped the timing of dyngo-4a and pitstop-2 action. The time of action for dyngo-4a and pitstop-2 largely overlapped with that of the reverse transcriptase (RT) inhibitor, azidothymidine (AZT) (Fig 1A) and thus was not consistent with the HIV entry inhibitor Maraviroc (an early acting CCR5 receptor antagonist) (Fig 1A). This observation supports that dynamin and clathrin act at a common viral post-entry point in HeLa cells that is unrelated and potentially additional to the initial HIV entry/fusion event. As the observed block by both dyngo-4a and pitstop-2 was late, we could not rule out an additional entry block mediated by either compound.

Given the unexpected profiles in time of addition assays, our focus turned to resolving the site(s) of dynamin and clathrin action in more detail not only in HeLa cells, but also using assays compatible with primary activated CD4 T cells. Activated T cells were initially used in time of addition assays to pinpoint dynamin blocks across the entire HIV life cycle, as they sustain productive HIV infection (resting CD4 T cells are not proliferative and HIV infection is largely transcriptionally silent). From our time of addition assays in HeLa cells and preliminary observations in HIV fusion assays in primary T cells, we were confident that 2 hours was sufficient for the completion of the HIV fusion reaction. Therefore, we consolidated time of addition assays to pre-entry (0 hours) and post entry/fusion (2 hours).

To mechanistically dissect the action of dynamin and clathrin inhibition in HeLa cells and primary T-cells, we combined this time of addition approach with detection of full length HIV DNA. The detection of accumulation of full length HIV DNA products during the HIV life cycle was then used to pinpoint any dynamin related blocks in the HIV life cycle from entry through to reverse transcription. For HeLa cells and activated CD4 T cells (Fig 1B-C) dyngo-4a inhibited full-length HIV DNA synthesis early (0 hours) but not late (2 hours), mirroring the action of the chemokine receptor entry inhibitors Maraviroc and AMD3100 (CCR5 and CXCR4 receptor

antagonists respectively) and diverging from that of the RT inhibitor AZT (Fig 1B-C). This demonstrates support for dynamin in virus entry but not reverse transcription, in both HeLa and activated CD4 T cells. For pitstop-2, we were restricted in observing only events in HeLa cells as short-term exposure of this compound to primary CD4 T cells led to significant loss of cells (a known limitation of this compound for some cell types<sup>47</sup>). In HeLa cells pitstop-2 significantly increased HIV DNA, whether added pre or post fusion events (Fig 1B), ruling out an endocytic block as the sole basis for interpreting dynamin's role. Overall, whilst dynamin and clathrin inhibition shared a common post-entry block in initial time of addition assays, we did not observe any evidence for a block at the level of reverse transcription using Q-PCR detection of full length HIV DNA. Furthermore, Q-PCR further revealed evidence that dynamin inhibition (and not clathrin) can lead to additional blocks at the level of HIV entry/fusion.

### ***Resolution of HIV post-entry blocks mediated by dynamin inhibition***

Given the complications of pitstop-2 in primary cells, we consolidated our observations using dynamin inhibition through dyngo-4a. The next series of experiments expanded our time of addition assays to pinpoint any blocks post reverse transcription using detection of HIV DNA in two specific states. The first was 2LTR HIV DNA circles that primarily forms within the nucleus and increases if HIV integration is blocked<sup>48,49</sup>. A decrease in 2LTR DNA post-HIV fusion would support a block in nuclear import, whilst an increase would support a block in integration. Secondly, we detected genomically integrated HIV DNA using Alu-HIV PCR<sup>50-52</sup> to confirm if HIV has successfully integrated into the human genome. In these assays, we incorporated the HIV integration inhibitor raltegravir as a control.

With the HeLa TZM-bl cell line, 2LTR DNA levels were not significantly lower or higher in the presence of dyngo-4a added at 2 h post-infection (Fig 2A,  $p = 0.182$ ;  $n = 4$ ). In contrast the HIV Integrase inhibitor Raltegravir significantly increase in 2LTR circles relative to both DMSO and dyngo-4a treatments (Fig 2A,  $p = 0.0044$  and  $p = 0.0043$  respectively;  $n = 4$ ). This suggests that dynamin does not have a role in the transport across the nuclear envelope or in HIV integration. Unfortunately, we could not carry out molecular assays that determine genomically integrated HIV copies as the TZM-bl cell line given it contains integrated copies of HIV LTR to drive  $\beta$ -galactosidase and luciferase expression. However, based on the 2LTR Q-PCR observations, we conclude that dynamin inhibition by dyngo-4a blocks the HIV life-cycle at a point after integration in the HeLa cell model.

Experiments were then extended to primary activated CD4 T cells. In activated CD4 T cell HIV 2LTR Q-PCR assays, the inhibitory profiles were similar to those in HeLa cells (Fig 2B). Furthermore, detection of integrated HIV DNA supported dyngo-4a to have no effect on HIV integration when added post entry (2 hours) (Fig 2C). Both observations do not support that dynamin inhibition results in blocks to HIV integration in activated T cells (as is the case in HeLa cells). As an index of HIV transcription in activated T cells, intracellular HIV p24 accumulation was then determined. When cells were exposed to dyngo-4a 2 hours post-infection (i.e. post-HIV fusion) a significant decrease in HIV p24 positive cells was observed (Fig 2D-E). Based on the cumulative evidence above, dynamin inhibition cannot block HIV integration but can lead to a block in active products in HIV infection (ie. transcription).

We then aimed to resolve why inhibition of dynamin would lead to a HIV transcriptional block. One mechanism of action that is consistent with dynamin inhibition and HIV transcriptional regulation<sup>53</sup> is its action on the cell cycle. Dynamin inhibition is known to directly influence cell cycle progression by arresting late stages of cytokinesis, when dynamin is specifically localised to the mid-body<sup>54</sup>. Similarly, inhibition of clathrin also blocks mitotic progression through its well-known moonlighting role at the mitotic spindle<sup>31</sup>. These mechanisms are consistent with both proteins mediating this post-entry effect. Therefore, the role of cell-cycle influences on HIV transcription was analysed. In single round TZM-bl HeLa infections, reverse transcription should proceed in the pool of cells at the S-G2-M stage of the cell cycle<sup>53,55,56</sup>, as the dNTP pool is increased, permitting efficient reverse transcription<sup>55,57</sup>. However, later HIV TAT dependent transcriptional activation requires entry into the G1 stage of the cell cycle<sup>45</sup>. To identify potential changes to the cell cycle in the presence of dyngo-4a the HeLa cell line FUCCI (Fluorescent ubiquitination-based cell cycle indicator) was used. These cells express two fluorescent protein tags, mKO2 to indicate the G1 phase, Geminin (amino acids 1-120) and Azami-Green 1 (mAG1) to visualize S, G2 and M phases<sup>58</sup> (Fig 2F). In unsynchronized FUCCI HeLa cells, dyngo-4a caused cells to accumulate in S-G2-M phase (Fig 2G). This is consistent with the hypothesis that the dyngo-4a block in HIV transcription is due to lack of G1 progression and subsequent lack of HIV TAT expression.

We searched for a similar cell-cycle related mechanism in activated CD4 T cells, where HIV transcription is known to be linked to cell cycle progression<sup>53</sup> and therefore HIV replication is primarily detected in daughter T cells. Activated T cells were loaded with Cell Trace Violet and cell division was quantified as accumulation of daughter cell populations. A complete ablation of all daughter cells was observed in the presence of dyngo-4a (Fig 2H). In the presence of dyngo-4a counter staining for the T cell activation marker CD25 and the viability dye 7-Aminoactinomycin D (7-AAD) confirmed that the T cells consisted of viable parent cells that had not divided and which retained high CD25 expression. This reveals that activated, proliferating CD4 T cells are susceptible to the effects of cytokinesis arrest driven by dynamin inhibition. Therefore, the mechanism of post-entry/fusion HIV inhibition involves a dynamin-dependent block in cell cycle progression and subsequent HIV transcriptional activation in different cell types and is independent from its role in endocytosis.

#### ***HIV endocytosis in primary resting CD4 T cells is limited***

In the above observations using detection of HIV reverse transcription products, we observed enhancement of HIV entry/infection by blocking clathrin and inhibition by blocking dynamin. This initial observation suggests a role for dynamin at the point of entry independent of HIV endocytosis. To provide alternative support for this observation, we simply observed whether the frequency of endocytosis in primary CD4 T cells correlated with HIV fusion kinetics and/or events. Previous studies have shown resting CD4 T cells have significantly lower levels of endocytosis compared to activated CD4 T cells<sup>59</sup>. We therefore correlated the extent of bulk endocytosis and CD4 receptor endocytosis in resting and activated T cells with HIV fusion. As resting CD4 T cells do not express the transferrin receptor<sup>60</sup>, traditional assays based on endocytosis of this receptor could not be employed. Therefore, assays utilizing membrane labelling by FM dyes were used. This approach has previously revealed

that activated T cells have 10-fold higher endocytosis rates than in resting T cells<sup>59</sup>. Consistent with this, we observed much lower levels and slower kinetics of endocytosis in resting than in activated cells (Fig 3A-B). Endocytosis in resting CD4 T cells resulted in the formation of only one to two small endosomes after 1 hour with the FM dye, while most of the activated T cell population accumulated a range of large FM-dye positive intracellular endosomal compartments within minutes (Fig 3A-B).

Since HIV initially binds to CD4 on the plasma membrane, and CD4 T cells can also negatively regulate CD4 endocytosis via tethering at the plasma membrane through the lymphocyte specific src kinase Lck, we further observed CD4-specific endocytosis using the CD4 mAb clone OKT4 conjugated to Alexa Fluor 488 (Fig 3C-D). OKT4 recognizes an epitope in the IgG domains 3 and 4 of CD4<sup>61</sup>, away from the HIV binding site in IgG domain 1<sup>62</sup>. Whilst in previous experiments we utilised R5 HIV isolates, it was important in all primary CD4 T cell assays, that we utilised the X4 tropic HIV isolate (in this case HIV<sub>NL43</sub>), as fusion is detected across both naïve (CD45RA<sup>+ve</sup>) and memory CD4 T cell subsets (CD45RA<sup>-ve</sup>) in addition to activated CD4 T cells, whilst R5 HIV fusion is restricted to only the memory and activated CD4 T cell sub-populations<sup>63</sup>. Using TIRF microscopy over time, planes were imaged proximal to, but beyond the plasma membrane. Resting CD4 T cells only slowly formed CD4-positive endosomes over 60 to 90 minutes, while a subpopulation of activated CD4 T cells (36%) exhibited a large accumulation of CD4 into endosomes (Fig 3C-D). To confirm that CD4 staining was within closed endosomal compartments pronase was used to cleave residual surface accessible CD4 and CD4-mAb (Fig 3E). After pronase treatment the internal CD4 mAb fluorescence was detected by flow cytometry and was again only elevated in a subpopulation of activated T cells. Therefore, by independent measures, resting T cells have a much lower overall and CD4 specific endocytic capacity than activated T cells.

HIV-1 entry was next examined in conjunction with CD4 endocytosis. HIV dynamics were visualised in live cells pulsed with fluorescent HIV particles, then incubated with the OKT4 Alexa Fluor 488 conjugated antibody. In resting CD4 T cells HIV was primarily detected at the cell periphery, with no or very limited detection of CD4-positive endosomes over the 60-minute period of live imaging (Fig 3F; Video S1). Whilst in activated CD4 T cells we readily observe HIV within CD4 positive endosomes after only a few minutes (Fig 3G; Video S1). The presence of virions in the activated CD4 T cell culture was not associated with a significant increase of CD4 positive endosomes in the absence or presence of HIV virions (39.6% +/- 17.23 versus 34.7% +/- 15.03%; n = 6 independent donors; p = 0.612). These observations reveal that low vs high CD4 endocytosis rates in resting and activated T cells, respectively, correlate with the extent of accumulation of HIV in endosomal compartments. The data also shows that HIV does not induce increased HIV endocytosis in primary CD4 T cells. Therefore, HIV can indeed enter endosomes, but this occurs at very low levels in resting CD4 T cells and only within a sub-population of activated CD4 T cells. However, this does not reveal whether HIV fusion and active infection can follow this entry to the endosomal system. Further, these initial combined observations do not support the idea that the timing of endocytosis in CD4 T cells supports HIV fusion, since endocytosis is so low in resting T cells and the kinetics.

### ***HIV kinetics and fusion rates are higher in resting CD4 T cells***

To assess whether the rates of endocytosis in activated T cells might increase HIV fusion by the accumulation of virions in endosomal compartments, we next correlated endocytosis rates with HIV fusion rates. Across independent donors, HIV fusion was consistently higher in resting versus activated T cells (Fig 4A;  $p = 0.024$ , which is in stark contrast to the relative endocytic capacities of the two cell populations (Fig 3).

The kinetics of early HIV events were then determined using the time taken for two distinct entry inhibitors to lose their antiviral activity: BMS806 blocks the initial envelope CD4 binding<sup>64</sup> and AMD3100 blocks subsequent binding to the chemokine receptor CXCR4<sup>65</sup>. Later stages of HIV fusion, after CD4 and chemokine receptor binding, were blocked by lowering the temperature below 20°C to reveal total fusion kinetics<sup>21,66</sup> (Fig 4B). In measuring the kinetics, our aim was to correlate any bottleneck in HIV attachment and/or fusion in cells with limited HIV endocytosis (resting T cells) versus their counterparts that actively engage in HIV endocytosis (activated CD4 T cells).

HIV engagement of its receptors CD4 and CXCR4, was faster in resting CD4 T cells compared to matched activated T cells (Fig 4C-D). Temperature blocking similarly revealed that resting CD4 T cells had faster overall HIV fusion kinetics (Fig 4C-D). Therefore, endocytosis of HIV is not a limiting step for HIV to initially engage its receptors and complete its fusion reaction in CD4 T cells.

#### ***HIV fusion in resting T cells is primarily at the plasma membrane***

The lack of a positive correlation between endocytosis rates and HIV fusion supports a model in which HIV fusion primarily occurs at the plasma membrane in resting CD4 T cells. To directly test this hypothesis, we determined surface accessibility of the HIV fusion reaction through surface pronase digestion. We focussed on the action of pronase on receptor cell surface accessibility, as stripping proceeds at temperatures that block endocytosis and HIV fusion (schematic presented in Fig 5A).

As a positive control for this assay, we attempted to use a virus pseudotyped with an endocytosis dependent viral envelope, Vesicular Stomatitis Virus Glycoprotein (VSVg). Unfortunately, we did not observe any difference in the pronase versus temperature block curves. Whilst this was initially unexpected, previous studies analysing the kinetics of VSVg fusion have reported that VSVg mediated fusion occurs within 2 minutes following endocytosis<sup>67</sup>. This process is consistent with our observations as we found that VSVg fusion proceeded almost immediately after the viral particle entered the endosomal network. In contrast, HIV fusion has a lag post receptor binding and in turn pronase assays can be used to detect endosomal fusion. Given the extensive viral endocytosis in HeLa cells, we utilised this cell type as an alternate positive control for this assay. Using this approach in HeLa cells, we found a significant proportion of fusion events being completed in a surface inaccessible compartment. This was revealed by the pronase treatment curve being left shifted relative to the overall fusion kinetics derived under temperature block conditions (Fig 5B).

After establishing the pronase assay using the HIV HeLa cell model as a positive control for the assay outlined in Fig 5, we applied similar conditions to primary CD4 T cells. In resting CD4 T cells the kinetics of HIV fusion in the presence of pronase was not significantly different at any time point to the overall kinetics of HIV fusion in the absence of pronase (Fig 5C). In activated CD4 T cells the extent of HIV fusion in the presence of pronase was slightly, but significantly, higher at the 30 and 60

minute time points (Fig 5D). This effect was subtle at both time points, but revealed a proportion of cells in which HIV fusion occurs through a surface inaccessible compartment. These pronase studies provide support for a proportion of HIV fusion events to proceed in a surface inaccessible compartment in activated CD4 T cells. In contrast, we found that the fusion reaction in resting CD4 T cells is entirely surface accessible, which is consistent with our observations of limited constitutive endocytosis and subsequent lack of viral particle endocytosis in this cell type. Thus, in resting CD4 T cells HIV fusion primarily proceeds at the plasma membrane, with no evidence for endosomal fusion. This does not support the hypothesis that fusion is dependent on HIV endocytosis and in turn dynamin's role in this latter process.

### ***Mechanisms that bias HIV fusion to the plasma membrane versus the endosome***

In contrast to our observations in resting CD4 T cells, HIV single particle tracking in HIV-HeLa models revealed a bias towards fusion in endosomes<sup>21,24</sup>. We next determined the mechanisms underpinning this bias. With respect to the process of HIV endocytosis, there are two key differences between resting CD4 T cells and HeLa cells (and/or non-lymphoid cells like macrophages) that can influence HIV fusion site. Firstly, constitutive endocytosis in HeLa cells far exceeds that of resting CD4 T cells. Secondly, the lymphocyte restricted Src kinase, Lck, tethers CD4 to the surface of T cells by non-covalent association with cytoplasmic domain of CD4<sup>68</sup> by preventing CD4 entry into clathrin-coated pits<sup>69</sup>. To determine if Lck expression can tether CD4 at the surface in the face of constitutive endocytosis, Lck was stably introduced into the engineered HeLa cell line TZM-bl and an Lck-positive population was clonally selected. TIRF imaging of CD4 dynamics in TZM-bl revealed high CD4 endocytosis rates (Fig 6A, C; Video S3 right video), as reported by others<sup>69,70</sup>. Introduction of Lck in TZM-bl-Lck cells almost abolished CD4 endocytosis (Fig 6B, C; Video S3 left video). HIV single particle tracking revealed HIV only entered CD4 positive endosomes in TZM-bl cells (Fig 6D; Video S4 right video). This accounts for the previous observations of endosomal fusion, as the high turnover of CD4 into endosomal networks in TZM-bl cells likely drives late stages of fusion within these compartments. Introduction of Lck in this setting tethers CD4 to the surface, as it does in CD4 T cells, shifting the fusion reaction to the plasma membrane. This highlights the importance of endocytic capacity and Lck-CD4 tethering as the primary influences of the HIV fusion site.

A reduction in CD4 endocytosis by CD4-Lck tethering to the plasma membrane would in turn drive the fusion reaction to the plasma membrane, as we have observed already in resting CD4 T cells. If this is the case in HeLa cells, this would support HIV fusion proceeding with similar efficiency at the plasma membrane and from within endosomes. Therefore, we determined if HIV fusion and subsequent infection proceeds in the TZM-bl-Lck line as in CD4 T cells. In infectivity assays, there was no significant difference between TZM-bl or TZM-bl-Lck cells (Fig 5F,  $p = 0.693$ ). In HIV fusion assays, TZM-bl-Lck cells showed non-significantly higher levels of HIV fusion (Fig, 6G,  $p = 0.561$ ) compared to parental TZM-bl cells. This dataset confirms our observations above in resting T cells: dynamin's potential role in HIV entry/fusion is unrelated to HIV particle endocytosis. Rather dynamin's endocytic role combined with Lck-CD4 tethering influences the site of HIV fusion in T cells. Whilst Lck is also present in activated CD4 T cells, the process of activation uncouples CD4-Lck tethering through a series of phosphorylation events<sup>71-74</sup>. This

combined with increased constitutive endocytosis culminates in a phenotype that also enables HIV endosomal fusion.

### ***Dynamin function in the HIV fusion reaction at the plasma membrane in CD4 T cells***

The controversy regarding the role of dynamin in HIV entry into endocytosis active cells such as HeLa and CD4 T cells can be clarified if dynamin plays two independent roles in this setting: one that regulates HIV particle endocytosis and a second role in the fusion reaction. These two roles are difficult to deconvolute in HeLa cells, as they proceed with similar rates/timing. Since endocytosis of HIV particles is slow and limited in resting CD4 T cells, this provides a unique platform that uncouples HIV fusion from viral endocytosis. The next series of experiments focussed on deciphering the role of dynamin in HIV fusion at the plasma membrane, and required the preceding comprehensive knowledge of HIV transcriptional blocks and HIV fusion bias to design the following assays and interpret their results.

We utilised the HIV fusion assay for two key reasons: Firstly, the HIV fusion assay allowed finer resolution and focus on early steps of HIV entry/fusion pathway; and secondly this enabled us to expand the study to dynamin's role in HIV fusion in not only bulk resting CD4 T cells, but across several CD4 T cell subsets by counter-staining cells with the lymph node homing marker CD62L and the naïve T cell marker CD45RA (Fig 7A-C). Using this approach, HIV fusion events using the X4 tropic isolate HIV<sub>NL43</sub> were found to occur across both naïve and memory CD4 T cell populations (CD45RA<sup>+ve</sup> & CD45RA<sup>-ve</sup>; Fig 7B). Inhibition of HIV fusion by dyngo-4a occurred at similar levels across all resting CD4 T cell subsets (Fig 7C). Significant inhibition of HIV fusion in resting and activated CD4 T cells was observed, with average maximal inhibition across four independent donors of 66.1% +/-2.66 versus 85.2% +/- 7.35 respectively (Fig 7D). Overall, both Q-PCR and HIV fusion assays independently reveal a dynamin-dependent block at the level of HIV fusion/entry in all cells examined. The results show that 1) HIV fusion is entirely surface accessible in resting CD4 T cells and thus confined to the plasma membrane, and that 2) dynamin is specifically involved in the fusion reaction occurring at the plasma membrane.

We next determined the kinetics of dynamin inhibition of HIV fusion in primary CD4 T cells by comparison with the action of HIV entry inhibitors BMS806 (CD4-HIV envelope binding), AMD3100 (chemokine receptor HIV envelope binding) and overall fusion using a temperature block. If dynamin directly influenced HIV fusion, finer mapping of the timing-of-inhibition should provide further insight into its potential role in the HIV fusion reaction. The data reveal that dyngo-4a inhibits HIV fusion shortly after chemokine receptor binding in both resting and activated CD4 T cell subsets (Fig 7E-F).

Dyngo-4a preferentially targets the GTPase activity of the lipid bound dynamin conformation associated with its helical oligomer. Dynamin is also known to exist a not-lipid bound conformation that is associated with the dynamin ring oligomer. To further dissect the role of dynamin in blocking HIV fusion in primary CD4 T cells, we utilised ryngo-1-23<sup>75</sup> a dynamin modulator class that promotes dynamin ring assembly. Time of addition experiments revealed ryngo-1-23 acted earlier than dyngo-4a in the HIV fusion reaction (Fig 7E-F), consistent with the two dynamin modulators having actions at different points in the dynamin oligomerisation cycle<sup>76,77</sup>. Further experiments using ryngo-1-23 and dyngo-4a in HeLa TZM-bl cell lines

generated equivalent inhibition of entry fusion profiles, supporting the timing of dynamin action around chemokine receptor binding is not restricted to only CD4 T cells (data not shown). Therefore, using distinct dynamin modulators, we found evidence to support dynamin's role both early and late in the HIV fusion reaction.

## Discussion

This study aimed to address the controversies surrounding dynamins role in HIV-1 fusion and identifying the HIV fusion site, by gaining a comprehensive understanding of dynamin's role in the entire HIV life cycle using different endocytosis modulators. In our systematic dissection in primary CD4 T cells and HeLa cell lines, we now observe a complex role for dynamin in influencing HIV infection. Our data supports three overall points of action for dynamin in HIV infection – one late role at the point of HIV transcription and two roles at the point of entry. The three roles are clearly mechanistically distinct and correlate with at least two previously reported cellular roles for dynamin in mitosis and endocytosis. In addition to the known and well characterised cellular roles of dynamin, we show that HIV fusion is dynamin-dependent at two discrete time points within the fusion pore lifetime that are independent of its functional role in viral endocytosis. These were revealed through use of dynamin modulators active against different conformational and/or oligomerisation states of dynamin, acting within the same mechanistic pathway.

Our study was primarily aimed towards understanding the actions of small molecule endocytosis inhibitors in the HIV life cycle. As previously reported for endocytosis modulators inhibiting mitosis in a non-endocytic manner<sup>31,37</sup>, we also observed a role for dynamin and clathrin late in the viral life cycle. For example, using HIV infection assays that detect events post-viral transcription we demonstrate significant inhibition of HIV infection by dynamin and clathrin inhibitors, at times-of-drug-addition that are temporally distinct from that of HIV entry/fusion. Resolution of the mechanism of action of dynamin inhibitors at this additional stage of the viral life cycle was shown to be a consequence of dynamin's influence on cytokinesis/cell cycle that, in turn, limited HIV transcriptional activity by blocking cell cycle progression. Whilst there were technical limitations when utilising pitstop-2 in primary T cells, its use supports a similar mechanism in proliferating HeLa cell lines. Firstly, the kinetics of post-entry inhibition using dyngo-4a and pitstop-2 are the same and secondly, both inhibition of dynamin and clathrin were previously shown to produce cell cycle arrest<sup>31,37</sup>. The observations show how caution is required before interpreting that a block in HIV infection is supportive of blocks to HIV entry/fusion, unless appropriate time kinetics are also considered.

In dissecting the role of HIV endocytosis in HIV fusion, we did not observe any positive correlation between HIV endocytosis and HIV fusion in CD4 T cells. Thus, we do not support HIV fusion/entry to be solely dependent on viral endocytosis and thus dynamin's role in this process. Rather viral endocytosis, and in turn dynamin's role in this setting, is to simply influence the probability of HIV fusion with an endosomal membrane. Observations across cell types reveals there is a continuum of viral endocytosis rates and as a direct consequence support or lack thereof for HIV endosomal fusion. At one extreme, we found that resting CD4 T cells have limited viral endocytosis and in turn lack endosomal fusion, with the plasma membrane being the preferred site of the HIV fusion reaction. At the other extreme, we observe HeLa cells with high levels of HIV endocytosis and evidence for fusion across endosomal membranes.

From the data in resting CD4 T cells, we conclude that any block of HIV fusion generated by dynamin inhibition is consistent with a role for dynamin in the HIV fusion reaction, irrespective of the fusion site. Therefore, we propose the third and potentially primary role for dynamin: i.e. influencing the HIV fusion reaction, independent of viral endocytosis. Evidence supporting a direct role for dynamin in the HIV fusion reaction is from four levels. First, when we consider the actions of clathrin inhibitors versus dynamin inhibitors in endocytosis versus HIV entry/fusion. For instance, the clathrin inhibitor pitstop-2 blocks endocytosis, but in Q-PCR assays it enhanced early HIV infection events using Q-PCR assays. Therefore, blocking endocytosis via an alternative target not related to dynamin does not negatively impact HIV entry. Second, ryngo-1-23 is reported not to block endocytosis<sup>34,78-80</sup> but blocks the early stages of the HIV fusion reaction. Third, although dyngo-4a has the potential to block endocytosis and HIV fusion simultaneously, the timing of its action is not consistent with endocytosis rates across resting and activated CD4 T cells. For instance, dyngo-4a action occurs at an earlier point in resting CD4 T cells (with slow endocytosis rates) than observed in activated CD4 T cells (with fast endocytosis rates). Finally, recent studies using dominant negative dynamins enabled the generation of CD4 T cell lines that failed to endocytose HIV particles, yet permitted HIV fusion and subsequent infection<sup>25</sup>. This study is consistent with our data in resting CD4 T cells: HIV fusion can proceed independent of HIV particle endocytosis. Whilst the data using dominant negative dynamins are supportive in this context, the fact they do not inhibit HIV fusion and/or later infection appears at odds with our observations of entry and post entry inhibition using dynamin inhibitors. This inconsistency can be reconciled with the potency of dynamin inhibition using small molecules versus the expression of dominant negative dynamins. For instance, the IC<sub>50</sub> of dyngo-4a for endocytosis is 5.7 μM, whilst its IC<sub>50</sub> for HIV fusion is 28 μM. Thus, at 10 μM dyngo-4a, cellular endocytosis can be blocked, but HIV fusion and subsequent infection can proceed at levels not significantly different to DMSO vehicle controls.

What might be the mechanism of dynamin's contribution to the HIV fusion reaction? Previous studies proposed a role for dynamin in endocytosis and also HIV pore dilation<sup>24,26</sup>. Whilst these studies are important, their interpretation was complicated by the cell type and the compound used to modulate dynamin's action. For instance, dynamin's dual influence on endocytosis and HIV fusion at the same rate in HeLa cells led to the conclusion HIV fusion was endocytosis dependent<sup>21,24</sup>. Compounding this is the use of dynasore, which has the ability to bind different dynamin conformation states and potentially co-influence the dynamics of ring and helical dynamin oligomers (46). Importantly, our study has enabled the re-interpretation of dynamin's role in HIV fusion by generating clarity at two levels: Firstly, we have demonstrated the role of dynamin in the HIV fusion reaction independent of endocytosis through our data in resting CD4 T cells. Secondly, we have incorporated well characterised dynamin modulators that preferentially act on distinct dynamin conformations: ryngo-1-23 by promoting dynamin rings and GTPase activity and dyngo-4a by inhibiting dynamin helical GTPase activity.

Consolidating our data, we now re-interpret dynamin's role in the fusion reaction. To ensure clarity of dynamin's action we will consider resting CD4 T cells and the timing of action for ryngo-1-23 and dyngo-4a in this setting in the next two paragraphs.

Ryngo-1-23 promotes ring formation, ie stimulates dynamin self-oligomerisation<sup>34,35,80</sup> and in this study it blocks HIV fusion prior to chemokine receptor binding. Dynamin rings have been previously shown to modulate and increase actin polymerization by displacing the capping protein gelsolin from the barbed ends of actin filaments<sup>34,35,80</sup>. The modulation of gelsolin plays a critical role in the F-actin regulation of CD4/chemokine receptor dynamics that increases the probability of chemokine receptor engagement post CD4 binding<sup>39,40</sup>. Additional F-actin events have been observed in resting CD4 T cells post chemokine receptor binding/signalling mediated either through HIV envelope or chemokines<sup>39,41-44</sup>. However, the timing of ryngo-1-23 actions observed in our experiments suggests that dynamin is acting at a point pre-chemokine receptor binding (schematic Fig 8).

Dyngo-4a does not promote dynamin oligomerisation but inhibits pre-existing dynamin oligomers in helical conformations much more potently than dynamin ring conformations<sup>46</sup>. Importantly, the extent of HIV fusion inhibition by ryngo-1-23 and dyngo-4a are the same but the timing of action is different: Ryngo-1-23 pre, whilst dyngo-4a post chemokine receptor binding. A model consistent with these two key observations is both compounds target the same pathway, but the timing differs due to their distinct mechanism of action on different dynamin conformation states. For instance, in exocytic vesicle fusion, both ryngo-1-23 and dyngo-4a modulate the fusion pore in different ways, causing expansion or constriction, respectively<sup>76</sup>. For HIV, there may be a sequential regulation of the HIV fusion pore, where initial recruitment of dynamin (ryngo-1-23 sensitive) within a ring conformation participates in coordinating early events, whilst the latter oligomerization of dynamin into larger helical oligomers (dyngo-4a sensitive) participates in the final stages of fusion pore dilation (Fig. 8).

During revision of this manuscript, Jones and colleagues<sup>77</sup> contributed independent evidence for dynamin's direct role in the HIV fusion reaction via a dual action: establishing hemi-fusion early and later stabilizing the HIV fusion pore. Their data, using different methodological approaches, supports our conclusions that dynamin can act on two different stages of the HIV fusion pathway independent of HIV particle endocytosis (schematic Fig 8).

Overall, we have mapped three mechanistically independent roles for dynamin that can independently influence HIV infection. To resolve dynamin's action in HIV infection, a continuum of cell types, viral assays and modulation of two specific dynamin oligomeric pools/conformations was needed. Our approach provide an in depth model of its action at the level of pre and post viral entry and suggest a re-interpretation of dynamin's role in HIV infection that addresses recent controversies regarding the HIV fusion site and presents a novel role for dynamin in viral fusion pore dynamics.

## Materials and Methods

### *Culture of CD4 T cells*

HEK F293T (Life Technologies) and TZM-bl (NIH AIDS Research and Reference Reagent Program) were grown in DMEM supplemented with 10% fetal calf serum (FCS). Primary CD4 T cells were isolated from whole blood as described previously<sup>81,82</sup>. Briefly, peripheral blood mononuclear cells (PBMCs) were isolated from whole blood (Australian Red Cross Blood service, Sydney) by density gradient centrifugation using Ficoll-Paque Plus (GE Healthcare, Little Chalfont, United Kingdom). CD4 T cells were either purified by negative selection directly from freshly isolated PBMCs using the CD4 T cell Isolation Kit II according to the manufacturer's instructions (Miltenyi Biotech). Cells were subsequently cultured at a density of  $2.5 \times 10^6$  cells.ml<sup>-1</sup> in RPMI 1640 supplemented with 2% human AB serum and 20 U.ml<sup>-1</sup> IL-2. CD4 T cells were activated with a cocktail of human anti-CD2 / anti-CD3 / anti-CD28 microbead conjugated particles (Human T cell activation kit II; Miltenyi Biotech) according to the manufacturer's instructions. The purity and activation status of CD4 T cells were determined by CD4, CD3, CD69 and CD25 surface staining and flow cytometric analysis with LSR-II flow cytometer (BD Biosciences).

### *Plasmids and virus stocks*

Viral particles expressing wild-type HIV-1 envelopes were based on the HIV<sub>NL4.3</sub> proviral vector. HIV-1<sub>BlaM</sub> expressing Vpr-BlaM *in trans* was generated by co-transfecting pNL4.3 and pmm310 (Vpr -  $\beta$ -lactamase chimeric protein) (Courtesy of Dr Michael Miller, Merck, USA via the AIDS Reagent Repository, NIAID, NIH, USA), while stocks of HIV<sub>NL4.3</sub> Vpr-mCherry that express Vpr-mCherry *in trans* were generated by co-transfecting pNL4.3 and pVpr-mcherry (Courtesy of Thomas Hope, Northwestern University, USA). HIV NL4.3 delta envelope (HIVdEnv) was generated by ligating the SalI to BamHI fragment derived from pHXB2-env (courtesy of Dr. A. Fisher and Dr. F. Wong-Staal via the AIDSreagent repository) into pNL4.3. VSVg envelope pseudotyping was carried out as previously described<sup>81,82</sup> using the pMDG.2 plasmid encoding VSVg (Courtesy of Didier Trono, via Addgene, MA, USA). HIV NL4.3 iGFP is a HIV construct where eGFP is expressed as a fusion protein within HIV Gag and developed as previously described<sup>81</sup>. Transfections for producing viral stocks were done in HEK F293T using polyethylenimine (at 1 mg.ml<sup>-1</sup> and neutralized to pH 7 (PEI Max, Polysciences, PA)) as described previously<sup>81,82</sup>. High-titre HIV-1<sub>BaL</sub> stocks were propagated in the SupT1-CCR5-CL.30 cell line as described previously<sup>83</sup>. Titering of viral particles was done on TZM-bl cell line as previously described<sup>83</sup>.

The TZM-bl line is a derivative of HeLa cells that were engineered by amphotropic retroviral transduction to express CD4 and CCR5, and which were later further engineered using a vector based on HIV-1 to contain Tat-responsive reporter genes for firefly luciferase and *Escherichia coli*  $\beta$ -galactosidase. The feature of this engineering renders them highly susceptible to HIV-1 infection in an easily quantifiable manner. In order to generate TZM-bl-Lck stable cell line, Lck ORF was amplified from pDONR223-Lck (Addgene #23890) using oligonucleotides AAAGAATTCATGGGCTGTGGCTGCAGC and

AAATCTAGATCAAGGCTGAGGCTGGTACTGG. Amplicons were then purified and shuttled into pLVXmCherryN1 expression vector (Clontech, Mountain View, CA) using *EcoRI/XbaI* restriction sites replacing the mCherry ORF with Lck. The resultant pLVX-Lck vector was co-transfected with helper plasmids psPAX2 and pHEF-Vsvg into HEK293T cells to generate lentivirus stocks as previously described<sup>81</sup>. TZM-bl cells were infected at a multiplicity of infection (MOI) of 1 and 7 days post-transduction high CD4 expressing cells were sorted into 96 well plates using a FACSaria (BD Biosciences). High CD4 expression was used as a surrogate marker for Lck as CD4 has been shown to couple with Lck<sup>56</sup>. Lck expression in selected clones was subsequently confirmed by immunostaining cells with mouse monoclonal anti Lck antibody (Santa Cruz Biotech, Dallas, USA) and AlexaFluor-633-conjugated rabbit anti-murine IgG antibody (Invitrogen, Carlsbad, USA) prior to visualization with a DeltaVision ELITE microscope (GE Life Sciences, Sydney, Australia).

Susceptibility of TZM-bl and TZMbl-Lck to HIV infection was quantified by measuring  $\beta$ -galactosidase transcriptional activity as previously described<sup>83</sup> quantification on InCell Investigator (Version 1.6, GE Life Sciences, Sydney, Australia).

### ***Inhibitors***

Maraviroc, Raltegravir, Zidovudine/AZT and Indinavir Sulfate were obtained from the NIH AIDS Research and Reference Reagent Program. The CXCR4 antagonist AMD3100 and fusion inhibitor T-20 were from Sigma-Aldrich. To ensure optimal activity, T-20 was dissolved in 10% ammonium hydroxide solution and stocks stored at -80°C. CD4-gp120 binding inhibitor BMS-378806 was obtained from Selleckchem as a 10mM stock solution.

Dynamin inhibitors dyngo<sup>®</sup>-4a and ryngo-1-23 and the clathrin inhibitor pitstop<sup>®</sup>-2 were synthesised as previously described<sup>31,46,75</sup>. All small molecule inhibitors were resuspended at 30 mM in DMSO and stored for a maximum of 2 months at -80°C. Prior to use, 30 mM stocks were brought to room temperature for 60 minutes and then diluted further to 10 mM with DMSO. At 80  $\mu$ M of dyngo-4a and ryngo-1-23, the final DMSO concentration was 0.8%. All inhibitors were tested for toxicity using Alamar Blue (Thermofisher) under the duration and conditions outlined in each assay. At 80  $\mu$ M, there was no effect of cellular viability for dyngo<sup>®</sup>-4a and ryngo-1-23. As mentioned in the results herein there were limitations of using pitstop<sup>®</sup>-2 in primary T cells as the EC<sub>50</sub> was calculated to be 44 $\mu$ M.

### ***Constitutive and CD4-specific endocytosis***

Activated CD4 T cells were magnetically depleted of antiCD2/CD3/CD28 murine monoclonal antibody conjugated microbeads and further treated with Live/Dead cell removal kit (Miltenyi Biotech) to remove non-viable cells. Both resting and activated CD4 T cells (1.25x10<sup>6</sup> cells per condition) were then exposed to the membrane dye FM 4-64 (10  $\mu$  M, red fluorescence) (Life Technologies) in serum free media. Cells were added to adjacent wells of a Greiner Sensoplate<sup>™</sup> glass bottom 96 well plate (170  $\mu$  m glass thickness, Sigma-Aldrich) pre-coated with CellTak or poly-L-lysine and briefly centrifuged at 200xg to promote adherence. Fluorescent images were acquired on a heated CO<sub>2</sub> fitted microscope stage using a 60x 1.45NA objective on a DeltaVision ELITE deconvolution microscope. The Z-depth was maintained by

infrared hard-focusing correction (Deltavision Ultimatefocus) to prevent any Z-direction drift over time. At 90 minutes post dye exposure, volume stacks were acquired from both resting and activated T cells to reveal accumulative levels of endocytosis. For CD4 specific endocytosis, anti-human CD4 antibody, 1  $\mu\text{g}$  of Clone OKT4, Alexa 488<sup>®</sup> (StemCell Technologies) was used in place of FM 4-64. In the case of TZM-bl and TZMbl-Lck,  $1.25 \times 10^5$  cells per condition were seeded into adjacent chambers of a Greiner Sensoplate<sup>™</sup> glass-bottom 96 well plate and incubated at 37°C overnight prior to incubation with the anti-human CD4 antibody Clone OKT4.

In order to distinguish between total and internal fluorescence, resting and activated CD4 T cells were exposed to CD4 Antibody, Cy<sup>®</sup>7, PE conjugate (Clone RPA-T4) (Life Technologies) and either placed on ice or incubated for 90 minutes at 37°C. This antibody binds to the D1 domain of CD4 and is susceptible to cleavage by pronase. Cells were then treated with varying amounts of pronase (0.5-4  $\text{mg} \cdot \text{ml}^{-1}$ ) followed by fixation in 1.2% paraformaldehyde. Flow cytometry was performed using a BD LSRII flow cytometer and analysis done with FlowJo software (Version 9.4.9, Tree Star Inc, California, USA).

#### ***Single particle tracking of HIV in CD4 T cells by TIRF microscopy***

Activated and resting CD4 T cells ( $1.25 \times 10^5$  per condition) were spinoculated with HIV<sub>NL4-3</sub> Vpr-mCherry (MOI of 1) at 1,200xg for 1 h at 4°C. In adjacent wells, HIV particles were adhered to poly-l-lysine in the absence of cells to establish the emitted fluorescence from single viral particles. Excess virus was washed off and cells moved to poly-l-lysine coated Greiner Sensoplate<sup>™</sup> glass bottom 96 well plates. Cells were mixed with anti-human CD4 antibody, Clone OKT4, Alexa 488<sup>®</sup> and fluorescent images acquired over time on a Deltavision microscope using a 60x TIRF objective 1.49NA objective combined with TIRF excitation using 488nm and 561nm lasers. Activated and resting CD4 T cells were acquired at the same time, by point visiting across two adjacent wells in a 96 well glass bottom plate. The total duration of imaging was 90 minutes with 10-second intervals. The Z-depth was maintained by infrared hard-focusing correction (Deltavision Ultimatefocus) to prevent any Z-direction drift over time. In the case of TZM-bl and TZM-bl-Lck, 6000 cells per condition were cultured overnight in Greiner Sensoplate<sup>™</sup> glass bottom 364 well plates at 37°C prior to virus spinoculation. In the TZM-bl experiments HIV<sub>NL43</sub>-iGFP was used. As above HIV particles were adhered to poly-l-lysine in the absence of cells to establish the emitted fluorescence from single viral particles. Cells were then stained with anti-human CD4 antibody, Clone OKT4, Alexa 488<sup>®</sup> and images acquired as described above.

#### ***HIV fusion assay***

The kinetics of HIV entry into the cytoplasm of CD4 T cells was determined using a Vpr-BlaM fusion assay<sup>84</sup>. Briefly, cells ( $1 \times 10^6$  for resting and activated CD4 T cells or  $3 \times 10^4$  for TZM-bl and TZM-bl-Lck cells) were treated with vehicle Dimethyl sulfoxide (DMSO), dyngo-4a (80  $\mu\text{M}$ ), ryngo-1-23 (80  $\mu\text{M}$ ), AMD3100 (10  $\mu\text{M}$ ), BMS-378806 (10  $\mu\text{M}$ ) or T-20 (50  $\mu\text{g} \cdot \text{ml}^{-1}$ ) for 30 min at 37°C in media containing 1% human serum. Pitstop-2 was excluded from use in fusion assays, as it reduced CCF2-AM loading at low  $\mu\text{M}$  (>10  $\mu\text{M}$ ) concentrations in a dose dependent manner

in all cells used. Cells were then spinoculated with HIV-1<sub>BlaM</sub> (expressing Vpr-BlaM in *trans*) at 800xg for 1h at 12°C. The amount of HIV-1<sub>BlaM</sub> was determined by titration on both primary and HeLa cell lines. For primary cells, concentrations of HIV-1<sub>BlaM</sub> that resulted in 10% positive fusion events (30% was maximal) was used and this was approximately 50µl of viral supernatant per 1x 10<sup>6</sup> cells. In HeLa cells concentrations of HIV-1<sub>BlaM</sub> that resulted in 30% positive fusion events (90% was maximal) was used and this was approximately 5µl of viral supernatant per 2.5x 10<sup>4</sup> cells. Cells were chilled on ice and washed extensively with either cold RPMI 1640 with 2% human serum (HS) for primary cells or DMEM with 10% Fetal Calf Serum (FCS) for HeLa cell lines. Non-spinoculation conditions (identical volume of virus incubated at 4°C) were also initially used to demonstrate that the type of fusion (plasma membrane vs endosomal) was not influenced by spinoculation. Fusion was initiated by shifting to 37°C and stopped after different times by adding the inhibitors at concentrations described above or by placing the cells on ice (temperature block). To detect HIV-1 specifically released into the cytosol, cells were washed twice in CO<sub>2</sub>-independent media before incubating in 100 µl of CCF2-AM loading solution (1 µM and 100 µg/mL Pluronic-F127) (Life Technologies) for 1 h at 18°C in a refrigerated benchtop centrifuge. CCF2-AM is a cell permeable BlaM (β-lactamase) substrate that is rapidly cleaved by endogenous cytoplasmic esterase to the negatively charged form, CCF2, which is retained in the cytosol. Cells were then washed once with developing solution (2.5 mM probenecid/NaOH in CO<sub>2</sub> independent media supplemented with 10% Fetal Calf Serum (FCS) and L-glutamine) and incubated in the same buffer overnight at 18°C. Where indicated, cells were stained for 30 min at 18°C with a cocktail consisting of anti-human CD45RA PE-Cf594, CD25 PE-Cy7 and CD62L APC-Cy7 (diluted 1 in 25, BD Biosciences) and/or Live/Dead discrimination near infra-red dye (Life Technologies). Finally, cells were fixed with 1.2% paraformaldehyde at 18°C for 3 h and the conversion of the green CCF2 dye by Vpr-BlaM to its blue fluorescent product was determined by multi parameter flow cytometry on an LSRII flow cytometer and analysis performed using FlowJo software. In the case of TZM-bl and TZM-bl-Lck cells, acquisition was done using a Cytell high content microscope ((GE Life Sciences, Sydney, Australia). Prior to imaging, cells were further stained with the live cell nuclear stain NucRed Live 647 (Invitrogen, Carlsbad, USA). Using the 4x objective, 7 fields of view were collected per well (approximately 5000 cells) and blue/green and far red cells identified and counted using high content automated algorithms developed using InCell Investigator based on fluorescence intensity and target cell or nuclei size (GE Life Sciences, Sydney, Australia).

In experiments involving pronase treatment: Pronase was reconstituted in water at 20mg.ml<sup>-1</sup>, sterile filtered using a 0.22µm filter and then batches were tested separately in HeLa cells, resting and activated CD4 T cells for their ability to inactivate HIV at 4°C for 10 minutes in the context of primary T cells and 1 minute in the context of HeLa cells. Inactivation of HIV post pronase treatment was then verified by raising the temperature to 37°C for 90 minutes and then subsequently detecting HIV fusion. Pronase levels that inactivated HIV, maintained cellular viability as detected by 7-AAD exclusion staining and were permissive to CCF2 dye loading were chosen for experiments outlined in figure 4. For resting and activated CD4 T cells, this was 2mg.ml<sup>-1</sup> and 1 mg.ml<sup>-1</sup> of pronase respectively for 10 minutes at 4°C. For HeLa cells this was 1 mg.ml<sup>-1</sup> of pronase for 1 minutes at 4°C. For experiments outlined in figure 4 HeLa cells, resting and activated T cells were

spinoculated with HIV-1<sub>BlaM</sub> as described above. Unbound virus was washed off, the cells incubated at 37°C for indicated times and subsequently placed on ice. The plasma membrane-bound virions were digested pronase in serum-free media at abovementioned levels at 4°C for 10 or 1 minute. Thereafter, the enzyme was inactivated with either 40ul of FCS for HeLa cells or 40 µL of HS for primary T cells. HeLa cells were washed twice in DMEM with 10% FCS and primary cells twice in RPMI media with 2% HS. Cells were either left on ice or incubated for another 90 minutes at 37°C. The cells were then developed for the fusion assay as outlined above.

#### ***HIV inhibition and time of addition assays on HeLa cells***

The refractiveness of HIV infection to dyn2 inhibitors and antiretrovirals over time was examined in TZM-bl cells seeded in an opaque 96-well plate at a density of  $4 \times 10^4$  cells per well and incubated at 37°C for 16 h. Drug stocks (10x concentrated) were prepared in complete DMEM media with 5% FCS (v/v) and added to the plated cells at 1 in 10 dilution and incubated at 37°C for 30 min. Inhibitors were added at the following final concentrations: 100 µM for dyngo-4a and pitstop-2 and 10 µM for Maraviroc, AZT and Raltegravir. Following this, cells were infected with HIV-1<sub>BaL</sub> by spinoculating at 1,200xg for 1h at 4°C<sup>85</sup>. Drugs were added back to the medium at indicated time points following infection and cells returned to 37°C. At 24 h post-infection the medium was removed and changed to fresh medium containing Indinavir Sulfate (10 µM) and the cells cultured for a further 48 h. Infection was assessed by measuring β-galactosidase transcriptional activity as previously described<sup>83</sup>; and percentage infection was calculated by normalising all results to those of the ‘no drug’ control.

#### ***qPCR assays with dyn2 and HIV inhibitors***

TZM-bl cells were infected with HIV-1<sub>BaL</sub> or HIV-1<sub>NL43</sub> (MOI of 0.04) via spinoculation at 1,200xg for 60 min at 4°C. Both HIV-1<sub>BaL</sub> and HIV-1<sub>NL43</sub> viral stocks were subjected to DNase I treatment (30 U.mL<sup>-1</sup>, New England Biolabs) for 90 mins at 37°C. Inhibitory compounds were added at either 0 or 2 h post-infection and further incubated for 24 h before being harvested for DNA extraction. Activated CD4 T cells were infected with HIV-1<sub>Vpx+</sub> (MOI of 0.5) as described above and treated with inhibitory compounds at 0 or 2 h post-infection. DNA extraction for all cell types was carried out with a QIAGEN kit (QIAamp DNA blood and tissue kit; QIAGEN) according to the manufacturer’s instructions. The final concentration of inhibitors in the assay were as follows; 100 µM for dyngo-4a, 10 µM for Maraviroc, 10 µM for AZT, 10 µM for Raltegravir and 5 µM for AMD3100. All drugs were prepared in complete DMEM media with 5% FCS (v/v).

Quantification of total HIV-1 DNA was performed as described previously<sup>86</sup>. Primers and locked-nuclei acid probe used were as follows: Forward primer: 5’AGT GGG GGG ACA TCA AGC AGC CAT GCA AT 3’; Reverse primer: 5’TAC TAG TAG TTC CTG CTA TGT CAC TTC C 3’; Probe: 6-FAM-AT[C]A[A]T[G]AGGAA[G]CT[G]C-BHQ-1. Reactions were made up in a final volume of 20 µl that contained 10 µl of iQ SuperMix (Bio-Rad, California, USA), 250 nM each of forward and reverse primers and 125 nM of probe. A volume of 2 – 4 µl of DNA template was added to the reaction as determined by the DNA concentration,

to ensure that at least 40 ng of template DNA per sample was used. PCR reactions were analysed on an iQ5 real-time PCR machine (Bio-Rad) with the following cycling conditions: denaturation at 95°C for 3 min, followed by 50 cycles of 10 sec at 95°C and 30 sec at 60°C. Total DNA copies were extrapolated from a pNL4.3 or pBaL standard curve. Data were normalised to the amount of input DNA specific for each sample to represent copies per 100 ng of input DNA and expressed as percentage of DMSO control.

Quantification of HIV-1 2-LTR circles was performed as previously described<sup>50</sup>. Primers and locked-nuclei acid probe used were as follows: Forward primer: 5'GCT AAC TAG GGA ACC CAC TGC TTA AG 3'; Reverse primer: 5'ACT GGT ACT AGC TTG TAG CAC CAT CCA 3'; Probe: FAM-ACA[C]A[C]A[A]G[G][C]T-BHQ1. The reaction mix was prepared as described above and PCR reactions were analysed on an iQ5 real-time PCR machine with the following cycling conditions: 1 cycle at 95°C for 3 min, followed by 45 cycles of 95°C for 15 sec and 60°C for 1 min. Total 2-LTR circle copy numbers were extrapolated from a standard curve and data normalised to the amount of input DNA.

Quantification of integrated HIV-1 DNA was achieved using a nested PCR protocol to detect Alu-LTR copies, as previously described<sup>51</sup>. First round primers were as follows: Forward Alu primer 5'TCC CCA GCT ACT GGG GAG GCT GAG3' and reverse Alu primer 5'GCC TCC CAA AGT GCT GGG ATT ACA G3' with the HIV specific primer L-M667 5' ATG CCA CGT AAG CGA AAC TCT GGC TAA CTA GGG AAC CCA CTG3'. Second round primers and locked-nuclei acid probe used were as follows: Forward primer 5' ATG CCA CGT AAG CGA AAC T3'; reverse primer 5'GCT AGA GAT TTT CCA CAC TGA CTA A3'; Probe: 6-FAM-CAC AAC AGA CGG GCA CAC ACT ACT TGA-TAMRA. The first round of amplification was performed in a total volume of 20 µL, which contained 10 µL of iQ Supermix, 1 mM MgCl<sub>2</sub>, 300 nM each forward and reverse Alu primers, 100 nM of L-M667 and 2 µL of DNA template. Amplification was performed in a thermocycler (Eppendorf) with the following cycling conditions; 1 cycle at 94°C for 7 min; 12 cycles of 94°C for 30 sec, 60°C for 30 sec and 72°C for 3 min; followed by 1 cycle at 72°C for 7 min. The amplified product was either used immediately or stored at 4°C for up to 24 hrs. The second round PCR reaction was performed in a 20 µL volume, which contained 10 µL of iQ Supermix, 1 mM MgCl<sub>2</sub>, 300 nM each of primer, 200 nM of probe and 2 µL of the amplification product generated in the first round to serve as the template. Amplification was performed in an iQ5 real-time PCR machine (Bio-Rad) with the following cycles conditions; 1 cycle at 95°C for 5 min, followed by 45 cycles of 95°C for 15 sec and 60°C for 1 min. Copies of Alu-HIV-1 were extrapolated from an ACH-2 standard curve (section 2.14.7) and data normalized to the amount of input DNA specific for each sample. Total integrated HIV DNA was extrapolated from a standard curve generated using the ACH2 cell line and data normalized to the amount of input DNA.

#### ***Post entry inhibition in activated CD4 T cells***

Resting CD4 T cells ( $1 \times 10^6$  per condition) were infected with HIV-1<sub>vpx</sub> by spinoculating at 800 x g for 1h at 12°C. At 24 hours post virus spinoculation cells were activated using Miltenyi Biotech cell expansion kit and dyngo-4a (100 µM) or DMSO added. At 72 h post infection cells were stained with CD25-APC (4 in 100) (BD Biosciences) followed by fixation and permeabilization in BD

Cytofix/Cytoperm™ Fixation and Permeabilization Solution. Cells were subsequently stained for intracellular HIV-1p24 (KC57-RD1 clone, Beckman Coulter, Miami, FL, 4 in 100) as described previously<sup>81</sup> and analysed by flow cytometry.

### ***Cell cycle progression***

FUCCI cells ( $5 \times 10^4$  per condition, Amalgaam, Japan) were seeded overnight in a 6-well plate then the cells were serum starved for 2 h before treatment with DMSO or dyngo-4a (100  $\mu$ M) for 48 h at 37°C. Cells were harvested and fixed in 4% formaldehyde and analysed via flow cytometry for mKO2 (red; 610 nm) and mAG (green; 525 nm) expression.

Freshly isolated CD4 T cells were and labelled with Cell Trace Violet (5  $\mu$ M) (Life Technologies) for 20 min at room temperature in the dark, in a volume of 1 mL phosphate buffered saline (PBS) (maximum  $10 \times 10^6$  cells). Cells were activated using the Miltenyi Biotech cell expansion kit as described above. DMSO or dyngo-4a was added 24 h post-activation at a final concentration of 100  $\mu$ M and cells incubated at 37°C for a further 48 h. At 72 h post-isolation the cells were washed in PBS supplemented with 1mM EDTA and 1% human serum (v/v) and stained for flow cytometry analysis using CD25-APC (diluted 4 in 100, BD Biosciences) and 7-AAD (50  $\mu$ g.ml<sup>-1</sup>, Sigma-Aldrich).

### ***Statistical analysis***

OriginPro (Version 9.0; Originlab Corporation, MA) was used to perform statistical analyses and generate graphs, unless otherwise specified. Unless otherwise stated, the data from two groups were compared, normal distributions were tested using a Shapiro-Wilk test and for normally distributed data the probability that the mean of each group was significantly different was evaluated using an unpaired student t-test. For data that is not normally distributed, the probabilities were determined using the Mann-Whitney U test.

### ***Acknowledgments***

This work was supported by a grant awarded by The Australian Centre for HIV and Hepatitis Virology Research (*ACH<sup>2</sup>*) (SGT & PJR), NHMRC Career Development Fellowship (SGT), NHMRC Research Fellowship (GNT1047070, PJR) and NHMRC project grants GNT1046703 (SGT) and GNT1105666 and GNT1069493 (PJR). We thank Professor Anthony Kelleher and Associate Professor Fabienne Brilot-Turville for their help in reading and editing of this manuscript.

Some of the authors' institutions (PJR & AM), Newcastle Innovation Ltd and Children's Medical Research Institute, hold trademarks for the Dynole, Dyngo and Rynngo compounds and make the compounds commercially available via Abcam (Cambridge, UK).

## Figure Legends

### **Figure 1. Small molecule inhibition of dynamin observes HIV inhibition profiles consistent with entry and post-entry**

(A) Time-of-drug-addition curves reveals that HIV becomes insensitive to drug action over time. The upper schematic summarises the time at which compounds were added following infection. The data for HIV infection is shown as a percentage of total infection after normalizing to the 'no drug' control and is representative of >5 independent experiments. (B-C) qPCR for full length HIV DNA. TZM-bl HeLa cells ( $2 \times 10^5$ ) were infected with the CCR5-utilising HIV-1<sub>Bal</sub> strain (B) or activated CD4 T cells with HIV-1<sub>NL43</sub> (C) in the presence of inhibitory compounds added at either 0 or 2 h post-infection. Data is expressed as mean and SEM and is representative of >3 independent experiments. \*  $p < 0.05$ , \*\*  $p < 0.01$ , \*\*\*  $p < 0.001$  compared to relevant DMSO control; unpaired Students t-test.

### **Figure 2: Resolution of HIV post-entry blocks through dynamin inhibition**

(A) Time-of-drug-addition and HIV 2LTR assays in TZM-bl cells (B) and primary activated CD4 T cells after HIV NL43 infections (as described in Fig. 1). qPCR was performed for HIV DNA 2LTR circles (A-B) to reveal potential blocks of nuclear transport and for HIV integrated DNA (C) to reveal any further blocks in genomic integration. The inhibitors were used at the following concentrations: Maraviroc (10  $\mu$ M), AZT (10  $\mu$ M), dyngo-4a (80  $\mu$ M), AMD3100 (5  $\mu$ M), Raltegravir (10  $\mu$ M). Data are representative of in excess of 6 independent experiments. \*  $p < 0.05$ , \*\*  $p < 0.01$ , \*\*\*  $p < 0.001$  with respect to relevant DMSO control; unpaired t-test. (D-E) Intracellular HIV p24 accumulation an index of productive HIV replication. Resting CD4 T cells were initially infected with NL43 and 2 hours later cells were activated and dyngo-4a was added with relevant DMSO controls. At day 3 post infection, cells were permeabilized and stained for intracellular HIV p24. Data is representative of >3 independent experiments. \*\*\*  $p < 0.001$  compared to the relevant DMSO control; unpaired t-test. (F-H) The effects of dynamin inhibition on the cell cycle in HeLa FUCCI cells (F-G) and activated CD4 T cells (H). In (F-G), the fluorescent cell cycle indicator cells, FUCCI cells, express fluorescent proteins that change from green (mAG fluorescent protein) to red (mKO2 fluorescent protein) throughout key points during the cell cycle detected by flow cytometry for expression of mKO2 (red; 610 nm) and mAG (green; 525 nm). Quantification of discrete stages of the cell cycle in FUCCI cells are presented in several flow cytometry gates. Red populations (mKO2<sup>+ve</sup>) are gated as G1, yellow (mKO2<sup>+ve</sup>, mAG<sup>+ve</sup>) as G1-S transitioning cells and green (mAG<sup>+ve</sup>) as S-G2-M cells (H) Quantitation of primary CD4 T cell division via dilution of Cell Trace Violet to reveal daughter cell populations. Freshly isolated cells were stained with Cell Trace Violet (5  $\mu$ M) for 20 min then activated as outlined in Fig 1. Dyngo-4a (80  $\mu$ M) was added at 24 h post-activation and cells were harvested after 72 h to allow sufficient cell division and counter stained for flow cytometry using CD25-APC. The data was gated for live cells using 7-AAD dye exclusion. Cell division was determined by the left two quadrants where Cell Trace Violet is diluted through cell division (staining in the left quadrants is representative of CD4 T cell daughter cells). CTV; Cell Trace Violet. Data is representative of 3 independent donors.

**Figure 3. HIV endocytosis in primary resting CD4 T cells is limited and is increased through T cell activation**

(A-D) CD4 T cells isolated from fresh blood were activated or not by anti CD2/CD3/CD28 murine monoclonal antibody conjugated microbeads for 48 hours. Fluorescent images were acquired on a heated CO<sub>2</sub> fitted microscope stage using a 60x 1.45NA objective on a DeltaVision ELITE deconvolution microscope, with activated and resting CD4 T cells acquired at the same time, by point visiting across two adjacent wells in a 96 well glass bottom plate (glass at 170 μm thickness). (A) Live cells were imaged over time in the presence of FM 4-64 (10 μM) in serum free media. After 90 minutes exposure to the dye, volume stacks were acquired to reveal cumulative levels of endocytosis and representative fields of view are shown. Scale bar is at 25 μm. (B) Kinetics of FM 4-64 endosomal accumulation in activated versus resting CD4 T cells over a 2 h live cell experiment. (C) CD4-specific endocytosis observed under similar conditions as in panel A, using a CD4 mAb OKT4 Alexa Fluor 488 conjugate instead of FM4-64. Representative fields of view. Scale bar is at 25 μm. (D) Quantitative endocytosis of CD4-Alexa-488 after 90 minutes shown as arbitrary fluorescence units (AU) of regions of interest for >70 activated and resting CD4 T cells derived from 3 independent donors. The red line is set above the highest value observed in resting CD4 T cells. (E) Flow cytometry compares the total CD4 fluorescence (no pronase) versus internalised fluorescence (pronase treated at 2 mg.ml<sup>-1</sup>) in resting CD4 T cells vs activated CD4 T cells. Flow cytometry gates are set once again based on the highest internal fluorescent signal in resting CD4 T cells. Percentage frequencies of cells above this threshold are presented in the lower right hand corner of each established gate. (F-G) Both resting (F) and activated CD4 T (G) cells were exposed to HIV<sub>NL4-3</sub> at 4°C for 2 h carrying the fluorescent marker Vpr-mCherry in trans at 4°C for 2 h. Excess virus was washed from cells and cells were moved to glass bottom plates (170 μm thickness) plates, previously coated with poly-L-Lysine. Cells were then mixed with the CD4 OKT4 Alexa Fluor 488 conjugated mAb and then briefly centrifuged at 200xg for one minute to promote adherence to the poly-L-Lysine coated wells. Fluorescent images were then acquired over time on a heated CO<sub>2</sub> fitted microscope stage using a 60x TIRF 1.49NA objective combined with TIRF excitation using 488nm and 561nm lasers on a DeltaVision ELITE deconvolution microscope. Images for resting and activated CD4 T cells were acquired at the same time, by point visiting across two adjacent wells in a 96 well glass bottom plate. The total duration of imaging was 90 minutes with 10 second intervals. One single Z-depth was maintained by infra-red hard-focusing correction (Deltavision Ultimatefocus) over time to prevent any Z-direction drift over time. Representative images are taken from videos s1 and s2 in the supplementary materials and methods. Arrows in both (F) and (G) highlight the representative positions of virions over time. For resting CD4 T cells (F) this is primarily at the plasma membrane and (G) with CD4 positive endosomes in a subset of activated CD4 T cells.

**Figure 4. HIV fusion kinetics in resting and activated CD4 T cells**

(A) Paired resting and activated CD4 T cells from 5 independent donors, D1 to D5, were subjected to HIV-1 fusion assays after exposure to HIV<sub>NL43</sub> carrying Vpr-BlaM at 4°C for 2 h, washing, and incubation for 2 hours at 37°C to allow completion of HIV fusion. Cytosolic virus was detected with the cytosolic BlaM substrate CCF2 overnight at 18°C. Data are means and standard deviations for duplicates from each

donor. **(B)** Model of site of action of HIV entry inhibitors. **(C-D)** The kinetics of HIV fusion in paired resting **(C)** and activated **(D)** CD4 T cells. The X-axis represents time in minutes when the drug is added or condition applied. The Y-axis is the actual % fusion positive cells detected over time. Numbers above arrows represent the time (min) when 50% of the total HIV fusion events (determined in 90 minute viral incubation without drug) are not sensitive to that drug or condition. Data from one donor in duplicate and is representative of 4 independent donors.

**Figure 5. HIV is surface accessible in resting CD4 T cells throughout the duration of the fusion reaction**

**(A)** Schematic of the HIV-pronase surface accessibility assay. In this pronase assay approach, there are two steps: i) cells are “temperature blocked” by transfer back to ice to stop all fusion and endocytosis events, virions on the plasma membrane are then digested with pronase (red scissors) and subsequent HIV fusion is measured. ii) Cells are transferred back to 37°C for another 2 h, to allow for fusion of only virions that had been internalized and thus protected from pronase, “pronase chase”.

**(B-D)** Using the scheme in **(A)**, **(B)** Positive control for the assay :HeLa-TZM-bl cells, resting **(C)** and activated **(D)** CD4 T cells were infected with HIV<sub>BlaM</sub>. Two experiments followed. Plasma membrane-bound virions were digested with pronase (2 mg.ml<sup>-1</sup> for resting T cells and 1 mg.ml<sup>-1</sup> for activated and HeLa cells), in serum-free media containing 20 mM HEPES) for 10 minutes at 4°C or cells were “Temperature Blocked” by remaining on ice for the remainder of the experiment. “Pronase” treated cells were then transferred back to 37°C to ensure the total time at 37°C was 90 minutes. All sets of cells were then developed for the fusion assay. Relative fusion is presented as a percentage of the total fusion at 90 minutes post infection (absolute fusion rates (denominator) in untreated controls at 90 minutes are approximately 10% for primary cells and 30% for HeLa cells). Data is expressed as mean and standard deviation of n = 5 replicates and for primary T cells is representative of at least 5 independent matched resting and activated CD4 T cell donors. \* = p<0.05, \*\*p<0.01 compared for temperature block versus pronase treatments; unpaired Students t-test.

**Figure 6. Role of Lck in CD4 plasma membrane tethering in HeLa cells**

CD4 trafficking dynamics in **(A)** TZM-bl (Lck negative) and **(B)** TZM-bl-Lck (Lck positive) HeLa cells. TZM-bl cell lines were analysed by real-time TIRF microscopy as in Fig 2 for 60 mins following application of AlexaFluor-488-conjugated OKT4 CD4 antibody. Accumulation of CD4-containing endosomes is shown at the indicated time points in one z-plane. Scale bars are 25 µm. **(C)** Quantification of CD4-containing endosome accumulation over time. Data are mean ± standard deviation of CD4 endosome accumulation per cell for 10 randomly selected cells. Data representative of 3 independent experiments **(D)** TZM-bl and **(E)** TZM-bl-Lck cells were infected with HIV<sub>NL43</sub>-iGFP prior to the addition of AlexaFluor-647-conjugated OKT4 CD4 antibody. Data represents virion internalisation events in 14 individual cells for each cell line per field of view. Virion-endosome colocalisation events were defined as contiguous pixels within the cytosol with overlapping fluorescence intensities. **(F)** TZM-bl and TZM-bl-Lck infection assays. Cells were incubated with varying amounts of HIV<sub>NL43</sub> for 4 days then HIV transcriptional activity was detected by X-gal staining of β-galactosidase-positive cells. Data are

mean X-gal (blue) positive cells across each well  $\pm$  standard deviation of triplicates wells. (G) TZM-bl and TZM-bl-Lck HIV fusion assay. Cells in glass bottom plates infected with HIV<sub>BLAM</sub> as outlined in Fig. 5. All data presented above is representative of 3 independent experiments. Scale bars in images (A-B) are 25  $\mu$ m.

**Figure 7. Dynamin inhibition blocks HIV fusion across cell types**

(A-D) Resolution of the role of dyn2 in HIV fusion across all cells using the HIV fusion assays. (A-B) Flow cytometry plots demonstrate representative resting CD4 T cell sub-populations analysed in this study based on CD62L staining (Y-Axis) versus the naïve marker CD45-RA staining (x-axis). This reveals 4 resting CD4 T cells populations, that are subsequently defined as central memory (Q1 = CD62L<sup>+ve</sup>CD45RA<sup>-ve</sup>), naïve (Q2 = CD62L<sup>+ve</sup>CD45-RA<sup>+ve</sup>), effector (Q3 = CD62L<sup>-ve</sup>CD45-RA<sup>+ve</sup>) and effector memory (Q4 = CD62L<sup>-ve</sup>CD45-RA<sup>-ve</sup>). Note total memory and naïve resting CD4 T cell populations can be grouped as simply CD45-RA<sup>-ve</sup> (left quadrants) and CD45<sup>+ve</sup> (right quadrants). (B) Representative HIV fusion is presented following the above gating of each resting CD4 T cell subset. HIV fusion is determined by the Vpr-BlaM catalysed conversion of the uncleaved CCF2 fluorescent antibiotic (y-Axis) to its blue cleaved derivative (x-axis and gated cell populations). (C) Summary of fusion inhibition in resting CD4 T cell subsets outlined in (A-B). Data is representative of at least 10 independent donors. (D) Summary of HIV fusion inhibition with the Dyn2 inhibitor dyngo-4a in primary CD4 T cell subsets versus HeLa cells (TZM-bl and TZM-bl-Lck). For (F-G) relative % HIV fusion is calculated by dividing values by the HIV fusion values in respective DMSO controls and x 100. Standard deviations are derived from the assay done in triplicate.

(E-F) Time of addition in conjunction with the HIV fusion assay to establish the timing of a dynamin ring modulator ryngo-1-23 versus a dynamin helices inhibitor - dyngo-4a. HIV entry inhibitors BMS806 blocks HIV envelope binding to CD4 and AMD3100 blocks chemokine receptor (CXCR4) binding. This establishes the timing of HIV- CD4 versus HIV-chemokine receptor binding respectively. The final steps of HIV fusion are revealed by temperature blocking of the fusion reaction. Total resting CD4 T cells (E) versus activated (F) CD4 T cells with ryngo-1-23 (blue) and dyngo-4a (red), are presented. Data is representative of 4 independent donors.

**Figure 8. Proposed HIV fusion blocks mediated by ryngo-1-23 and dyngo-4a**

Left: Ryngo-1-23 promotes the elongation of short F-actin through increasing the rate of dynamin ring oligomerisation. This in turn influences F-actin dynamics that are required for the receptor trafficking and which is a known pre-requisite for the commencement of HIV fusion (action pre-chemokine receptor binding). Right: Dyngo-4a preferentially inhibits dynamin activity after oligomerisation and in a distinct conformational form and prevents dynamin involvement in dilation of the HIV fusion pore (action post chemokine receptor binding).

**Video S1. Single particle HIV tracking in resting CD4 T cells**

Resting CD4 T cells were generated as outlined in Fig 3. Resting CD4 T cells were exposed to HIVNL43 at 4°C for 2 h carrying the fluorescent marker Vpr-mCherry. Excess virus was washed from cells and cells were moved to glass bottom (170  $\mu$ m

thickness) plates, previously coated with poly-L-Lysine. Cells were then mixed with the CD4 OKT4 Alexa Fluor 488 conjugated mAb and then briefly centrifuged at 200xg for one minute to promote adherence to the poly-L-Lysine coated wells. Fluorescent images were then acquired over time on a heated CO<sub>2</sub> fitted microscope stage using a 60x TIRF 1.49NA objective combined with TIRF excitation using 488nm and 561nm lasers on a DeltaVision ELITE deconvolution microscope. Scale bars indicate 25  $\mu$ m and image acquisition is approximately 1 frame per 10 seconds. Single z-planes over time are presented.

***Video S2. Single particle HIV tracking in Activated CD4 T cells***

Activated CD4 T cells were generated as outlined in Fig 3. Activated CD4 T cells were exposed to fluorescent HIV and the CD4 OKT4 Alexa Fluor 488 as described in the legend to Video S1. Activated T cells were derived from the same donor in Video S1 and images acquired in the well adjacent to the resting CD4 T cell population.

***Video S3. CD4 specific endocytosis in the TZM-bl HeLa cell line with and without Lck***

To observe CD4 trafficking dynamics in Lck-positive (Left movie) and negative TZM-bl cell lines (right movie), cells subjected to real-time TIRF microscopy over the period of 60 mins following the addition of AlexaFluor-488-conjugated OKT4 CD4 antibody. Scale bars indicate 25  $\mu$ m and image acquisition is approximately 1 frame per 10 seconds with a single z-plane presented.

***Video S4. Single particle HIV tracking in the TZM-bl HeLa cell line with and without Lck***

The Lck-positive (Left movie) and negative TZM-bl cell lines (right movie) were exposed to HIV NL43 at 4°C for 2 h carrying the fluorescent marker Vpr-eGFP. Cells were then mixed with the CD4 OKT4 Alexa Fluor 647 conjugated mAb. Cells were then imaged as outlined in the figure legend to Video S1. Note the appearance over time of HIV in CD4 positive endosomes Lck-negative cells.

## References

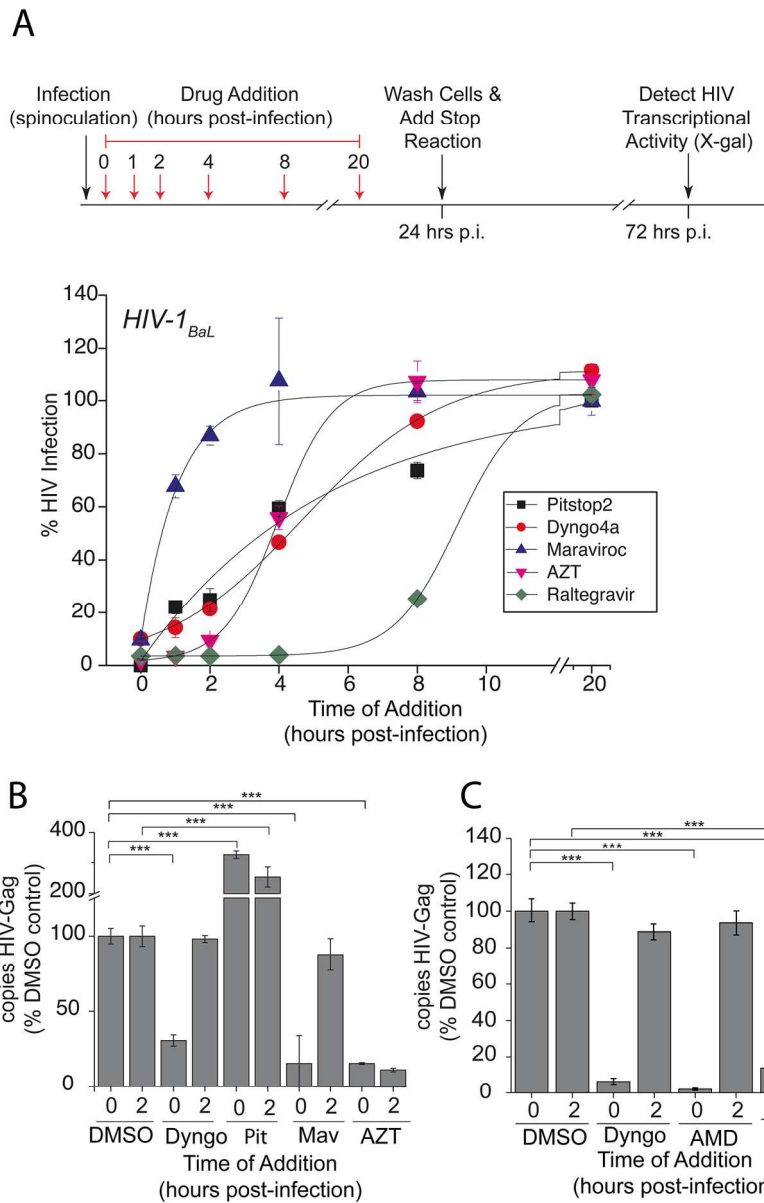
1. Lifson JD, Feinberg MB, Reyes GR, et al. Induction of CD4-dependent cell fusion by the HTLV-III/LAV envelope glycoprotein. *Nature*. 1986;323(6090):725-728.
2. Feng Y, Broder CC, Kennedy PE, Berger EA. HIV-1 entry cofactor: functional cDNA cloning of a seven-transmembrane, G protein-coupled receptor. *Science*. 1996;272(5263):872-877.
3. Alkhatib G, Combadiere C, Broder CC, et al. CC CKR5: a RANTES, MIP-1alpha, MIP-1beta receptor as a fusion cofactor for macrophage-tropic HIV-1. *Science*. 1996;272(5270):1955-1958.
4. Deng H, Liu R, Ellmeier W, et al. Identification of a major co-receptor for primary isolates of HIV-1. *Nature*. 1996;381(6584):661-666.
5. Dragic T, Litwin V, Allaway GP, et al. HIV-1 entry into CD4+ cells is mediated by the chemokine receptor CC-CKR-5. *Nature*. 1996;381(6584):667-673.
6. Choe H, Farzan M, Sun Y, et al. The beta-chemokine receptors CCR3 and CCR5 facilitate infection by primary HIV-1 isolates. *Cell*. 1996;85(7):1135-1148.
7. Doranz BJ, Rucker J, Yi Y, et al. A dual-tropic primary HIV-1 isolate that uses fusin and the beta-chemokine receptors CKR-5, CKR-3, and CKR-2b as fusion cofactors. *Cell*. 1996;85(7):1149-1158.
8. Wilen CB, Tilton JC, Doms RW. HIV: cell binding and entry. *Cold Spring Harb Perspect Med*. 2012;2(8).
9. Stein BS, Gowda SD, Lifson JD, Penhallow RC, Bensch KG, Engleman EG. pH-independent HIV entry into CD4-positive T cells via virus envelope fusion to the plasma membrane. *Cell*. 1987;49(5):659-668.
10. Maddon PJ, McDougal JS, Clapham PR, et al. HIV infection does not require endocytosis of its receptor, CD4. *Cell*. 1988;54(6):865-874.
11. McClure MO, Marsh M, Weiss RA. Human immunodeficiency virus infection of CD4-bearing cells occurs by a pH-independent mechanism. *The EMBO journal*. 1988;7(2):513-518.
12. Pauza CD, Price TM. Human immunodeficiency virus infection of T cells and monocytes proceeds via receptor-mediated endocytosis. *J Cell Biol*. 1988;107(3):959-968.
13. Pelchen-Matthews A, Clapham P, Marsh M. Role of CD4 endocytosis in human immunodeficiency virus infection. *J Virol*. 1995;69(12):8164-8168.
14. Pelchen-Matthews A, Signoret N, Klasse PJ, Fraile-Ramos A, Marsh M. Chemokine receptor trafficking and viral replication. *Immunol Rev*. 1999;168:33-49.
15. Fackler OT, Peterlin BM. Endocytic entry of HIV-1. *Curr Biol*. 2000;10(16):1005-1008.
16. Fredericksen BL, Wei BL, Yao J, Luo T, Garcia JV. Inhibition of endosomal/lysosomal degradation increases the infectivity of human immunodeficiency virus. *J Virol*. 2002;76(22):11440-11446.
17. Schaeffer E, Soros VB, Greene WC. Compensatory link between fusion and endocytosis of human immunodeficiency virus type 1 in human CD4 T lymphocytes. *J Virol*. 2004;78(3):1375-1383.
18. Daecke J, Fackler OT, Dittmar MT, Krausslich HG. Involvement of clathrin-mediated endocytosis in human immunodeficiency virus type 1 entry. *J Virol*. 2005;79(3):1581-1594.

19. Bosch B, Grigorov B, Senserrich J, et al. A clathrin-dynamin-dependent endocytic pathway for the uptake of HIV-1 by direct T cell-T cell transmission. *Antiviral Res.* 2008;80(2):185-193.
20. Clotet-Codina I, Bosch B, Senserrich J, et al. HIV endocytosis after dendritic cell to T cell viral transfer leads to productive virus infection. *Antiviral Res.* 2009;83(1):94-98.
21. Miyauchi K, Kim Y, Latinovic O, Morozov V, Melikyan GB. HIV enters cells via endocytosis and dynamin-dependent fusion with endosomes. *Cell.* 2009;137(3):433-444.
22. Uchil PD, Mothes W. HIV Entry Revisited. *Cell.* 2009;137(3):402-404.
23. Permanyer M, Ballana E, Este JA. Endocytosis of HIV: anything goes. *Trends Microbiol.* 2010;18(12):543-551.
24. de la Vega M, Marin M, Kondo N, et al. Inhibition of HIV-1 endocytosis allows lipid mixing at the plasma membrane, but not complete fusion. *Retrovirology.* 2011;8:99.
25. Herold N, Anders-Osswein M, Glass B, Eckhardt M, Muller B, Krausslich HG. HIV-1 entry in SupT1-R5, CEM-ss, and primary CD4+ T cells occurs at the plasma membrane and does not require endocytosis. *J Virol.* 2014;88(24):13956-13970.
26. Melikyan GB. HIV entry: a game of hide-and-fuse? *Curr Opin Virol.* 2014;4C:1-7.
27. van Wilgenburg B, Moore MD, James WS, Cowley SA. The productive entry pathway of HIV-1 in macrophages is dependent on endocytosis through lipid rafts containing CD4. *PLoS One.* 2014;9(1):e86071.
28. Herold N, Muller B, Krausslich HG. Reply to "Can HIV-1 entry sites be deduced by comparing bulk endocytosis to functional readouts for viral fusion?". *J Virol.* 2015;89(5):2986-2987.
29. Kondo N, Marin M, Kim JH, Desai TM, Melikyan GB. Distinct requirements for HIV-cell fusion and HIV-mediated cell-cell fusion. *J Biol Chem.* 2015;290(10):6558-6573.
30. Marin M, Melikyan GB. Can HIV-1 entry sites be deduced by comparing bulk endocytosis to functional readouts for viral fusion? *J Virol.* 2015;89(5):2985.
31. von Kleist L, Stahlschmidt W, Bulut H, et al. Role of the clathrin terminal domain in regulating coated pit dynamics revealed by small molecule inhibition. *Cell.* 2011;146(3):471-484.
32. Siliciano RF, Greene WC. HIV latency. *Cold Spring Harb Perspect Med.* 2011;1(1):a007096.
33. Hinshaw JE. Dynamin and its role in membrane fission. *Annu Rev Cell Dev Biol.* 2000;16:483-519.
34. Gu C, Chang J, Shchedrina VA, et al. Regulation of dynamin oligomerization in cells: the role of dynamin-actin interactions and its GTPase activity. *Traffic.* 2014;15(8):819-838.
35. Gu C, Yaddanapudi S, Weins A, et al. Direct dynamin-actin interactions regulate the actin cytoskeleton. *The EMBO journal.* 2010;29(21):3593-3606.
36. Itoh T, Erdmann KS, Roux A, Habermann B, Werner H, De Camilli P. Dynamin and the actin cytoskeleton cooperatively regulate plasma membrane invagination by BAR and F-BAR proteins. *Dev Cell.* 2005;9(6):791-804.
37. Chircop M, Perera S, Mariana A, et al. Inhibition of dynamin by dynole 34-2 induces cell death following cytokinesis failure in cancer cells. *Mol Cancer Ther.* 2011;10(9):1553-1562.

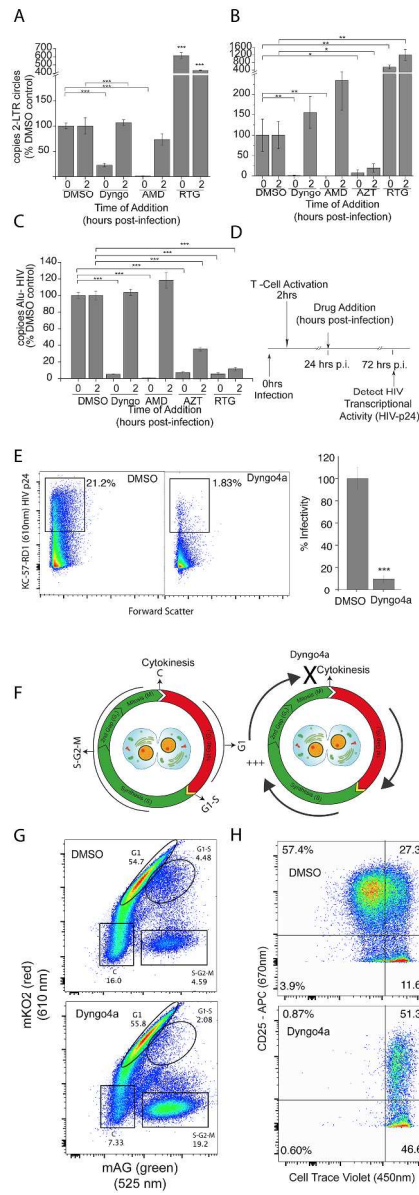
38. Smith CM, Chircop M. Clathrin-mediated endocytic proteins are involved in regulating mitotic progression and completion. *Traffic*. 2012;13(12):1628-1641.
39. Barrero-Villar M, Cabrero JR, Gordon-Alonso M, et al. Moesin is required for HIV-1-induced CD4-CXCR4 interaction, F-actin redistribution, membrane fusion and viral infection in lymphocytes. *J Cell Sci*. 2009;122(Pt 1):103-113.
40. Garcia-Exposito L, Ziglio S, Barroso-Gonzalez J, et al. Gelsolin activity controls efficient early HIV-1 infection. *Retrovirology*. 2013;10:39.
41. Pontow SE, Heyden NV, Wei S, Ratner L. Actin cytoskeletal reorganizations and coreceptor-mediated activation of rac during human immunodeficiency virus-induced cell fusion. *J Virol*. 2004;78(13):7138-7147.
42. Harmon B, Ratner L. Induction of the Galpha(q) signaling cascade by the human immunodeficiency virus envelope is required for virus entry. *J Virol*. 2008;82(18):9191-9205.
43. Yoder A, Yu D, Dong L, et al. HIV envelope-CXCR4 signaling activates cofilin to overcome cortical actin restriction in resting CD4 T cells. *Cell*. 2008;134(5):782-792.
44. Vorster PJ, Guo J, Yoder A, et al. LIM kinase 1 modulates cortical actin and CXCR4 cycling and is activated by HIV-1 to initiate viral infection. *J Biol Chem*. 2011;286(14):12554-12564.
45. Kashanchi F, Agbottah ET, Pise-Masison CA, et al. Cell cycle-regulated transcription by the human immunodeficiency virus type 1 Tat transactivator. *J Virol*. 2000;74(2):652-660.
46. McCluskey A, Daniel JA, Hadzic G, et al. Building a better dynasore: the dyngo compounds potently inhibit dynamin and endocytosis. *Traffic*. 2013;14(12):1272-1289.
47. Robertson MJ, Deane FM, Stahlschmidt W, et al. Synthesis of the Pitstop family of clathrin inhibitors. *Nat Protoc*. 2014;9(7):1592-1606.
48. Bukrinsky M, Sharova N, Stevenson M. Human immunodeficiency virus type 1 2-LTR circles reside in a nucleoprotein complex which is different from the preintegration complex. *J Virol*. 1993;67(11):6863-6865.
49. Farnet CM, Haseltine WA. Circularization of human immunodeficiency virus type 1 DNA in vitro. *J Virol*. 1991;65(12):6942-6952.
50. Koelsch KK, Boesecke C, McBride K, et al. Impact of treatment with raltegravir during primary or chronic HIV infection on RNA decay characteristics and the HIV viral reservoir. *AIDS*. 2011;25(17):2069-2078.
51. McBride K, Xu Y, Bailey M, et al. The majority of HIV type 1 DNA in circulating CD4+ T lymphocytes is present in non-gut-homing resting memory CD4+ T cells. *AIDS Res Hum Retroviruses*. 2013;29(10):1330-1339.
52. Swiggard WJ, Baytop C, Yu JJ, et al. Human immunodeficiency virus type 1 can establish latent infection in resting CD4+ T cells in the absence of activating stimuli. *J Virol*. 2005;79(22):14179-14188.
53. Wurtzer S, Compain S, Benech H, Hance AJ, Clavel F. Effect of cell cycle arrest on the activity of nucleoside analogues against human immunodeficiency virus type 1. *J Virol*. 2005;79(23):14815-14821.
54. Chircop M, Sarcevic B, Larsen MR, et al. Phosphorylation of dynamin II at serine-764 is associated with cytokinesis. *Biochim Biophys Acta*. 2011;1813(10):1689-1699.
55. Kootstra NA, Zwart BM, Schuitemaker H. Diminished human immunodeficiency virus type 1 reverse transcription and nuclear transport in

- primary macrophages arrested in early G(1) phase of the cell cycle. *J Virol.* 2000;74(4):1712-1717.
56. Korin YD, Zack JA. Progression to the G1b phase of the cell cycle is required for completion of human immunodeficiency virus type 1 reverse transcription in T cells. *J Virol.* 1998;72(4):3161-3168.
57. Pauls E, Ruiz A, Badia R, et al. Cell cycle control and HIV-1 susceptibility are linked by CDK6-dependent CDK2 phosphorylation of SAMHD1 in myeloid and lymphoid cells. *J Immunol.* 2014;193(4):1988-1997.
58. Sakaue-Sawano A, Kurokawa H, Morimura T, et al. Visualizing spatiotemporal dynamics of multicellular cell-cycle progression. *Cell.* 2008;132(3):487-498.
59. Fomina AF, Deerinck TJ, Ellisman MH, Cahalan MD. Regulation of membrane trafficking and subcellular organization of endocytic compartments revealed with FM1-43 in resting and activated human T cells. *Exp Cell Res.* 2003;291(1):150-166.
60. Pattanapanyasat K, Hoy TG. Expression of cell surface transferrin receptor and intracellular ferritin after in vitro stimulation of peripheral blood T lymphocytes. *Eur J Haematol.* 1991;47(2):140-145.
61. Jameson BA, Rao PE, Kong LI, et al. Location and chemical synthesis of a binding site for HIV-1 on the CD4 protein. *Science.* 1988;240(4857):1335-1339.
62. Arthos J, Deen KC, Chaikin MA, et al. Identification of the residues in human CD4 critical for the binding of HIV. *Cell.* 1989;57(3):469-481.
63. Dai J, Agosto LM, Baytop C, et al. Human immunodeficiency virus integrates directly into naive resting CD4+ T cells but enters naive cells less efficiently than memory cells. *J Virol.* 2009;83(9):4528-4537.
64. Madani N, Perdigoto AL, Srinivasan K, et al. Localized changes in the gp120 envelope glycoprotein confer resistance to human immunodeficiency virus entry inhibitors BMS-806 and #155. *J Virol.* 2004;78(7):3742-3752.
65. Schols D, Struyf S, Van Damme J, Este JA, Henson G, De Clercq E. Inhibition of T-tropic HIV strains by selective antagonization of the chemokine receptor CXCR4. *J Exp Med.* 1997;186(8):1383-1388.
66. Henderson HI, Hope TJ. The temperature arrested intermediate of virus-cell fusion is a functional step in HIV infection. *Virol J.* 2006;3:36.
67. Johannsdottir HK, Mancini R, Kartenbeck J, Amato L, Helenius A. Host cell factors and functions involved in vesicular stomatitis virus entry. *J Virol.* 2009;83(1):440-453.
68. Veillette A, Bookman MA, Horak EM, Bolen JB. The CD4 and CD8 T cell surface antigens are associated with the internal membrane tyrosine-protein kinase p56lck. *Cell.* 1988;55(2):301-308.
69. Pelchen-Matthews A, Boulet I, Littman DR, Fagard R, Marsh M. The protein tyrosine kinase p56lck inhibits CD4 endocytosis by preventing entry of CD4 into coated pits. *J Cell Biol.* 1992;117(2):279-290.
70. Pelchen-Matthews A, Armes JE, Griffiths G, Marsh M. Differential endocytosis of CD4 in lymphocytic and nonlymphocytic cells. *J Exp Med.* 1991;173(3):575-587.
71. Marie-Cardine A, Maridonneau-Parini I, Ferrer M, et al. The lymphocyte-specific tyrosine protein kinase p56lck is endocytosed in Jurkat cells stimulated via CD2. *J Immunol.* 1992;148(12):3879-3884.

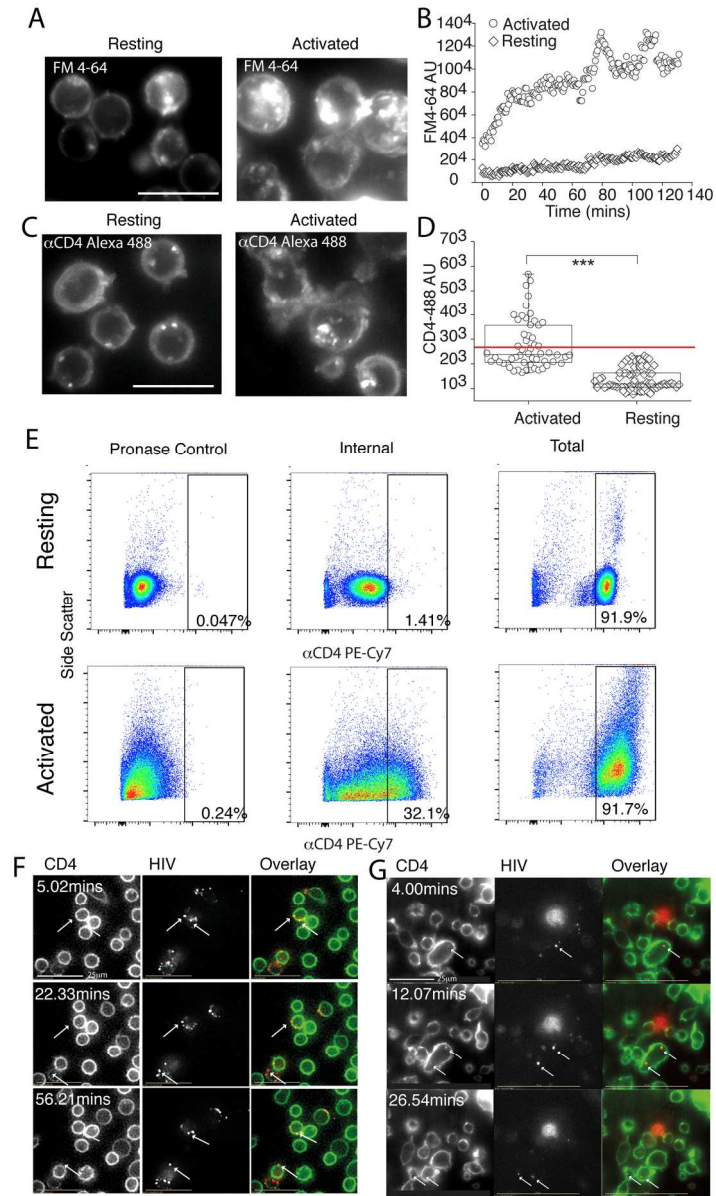
72. Chu K, Littman DR. Requirement for kinase activity of CD4-associated p56lck in antibody-triggered T cell signal transduction. *J Biol Chem.* 1994;269(39):24095-24101.
73. Veillette A, Horak ID, Horak EM, Bookman MA, Bolen JB. Alterations of the lymphocyte-specific protein tyrosine kinase (p56lck) during T-cell activation. *Mol Cell Biol.* 1988;8(10):4353-4361.
74. Hurley TR, Luo K, Sefton BM. Activators of protein kinase C induce dissociation of CD4, but not CD8, from p56lck. *Science.* 1989;245(4916):407-409.
75. Odell LR, Chau N, Mariana A, Graham ME, Robinson PJ, McCluskey A. Azido and diazarinyl analogues of bis-tyrphostin as asymmetrical inhibitors of dynamin GTPase. *ChemMedChem.* 2009;4(7):1182-1188.
76. Jackson J, Papadopulos A, Meunier FA, McCluskey A, Robinson PJ, Keating DJ. Small molecules demonstrate the role of dynamin as a bi-directional regulator of the exocytosis fusion pore and vesicle release. *Mol Psychiatry.* 2015;20(7):810-819.
77. Jones DM, Alvarez LA, Nolan R, et al. Dynamin-2 Stabilizes the HIV-1 Fusion Pore with a Low Oligomeric State. *Cell Rep.* 2017;18(2):443-453.
78. Lees JG, Gorgani NN, Ammit AJ, McCluskey A, Robinson PJ, O'Neill GM. Role of dynamin in elongated cell migration in a 3D matrix. *Biochim Biophys Acta.* 2015;1853(3):611-618.
79. Schiffer M, Teng B, Gu C, et al. Pharmacological targeting of actin-dependent dynamin oligomerization ameliorates chronic kidney disease in diverse animal models. *Nat Med.* 2015;21(6):601-609.
80. Sever S, Chang J, Gu C. Dynamin rings: not just for fission. *Traffic.* 2013;14(12):1194-1199.
81. Aggarwal A, Iemma TL, Shih I, et al. Mobilization of HIV spread by diaphanous 2 dependent filopodia in infected dendritic cells. *PLoS Pathog.* 2012;8(6):e1002762.
82. Turville SG, Aravantinou M, Stossel H, Romani N, Robbiani M. Resolution of de novo HIV production and trafficking in immature dendritic cells. *Nat Methods.* 2008;5(1):75-85.
83. Turville SG, Aravantinou M, Miller T, et al. Efficacy of Carraguard-based microbicides in vivo despite variable in vitro activity. *PLoS One.* 2008;3(9):e3162.
84. Cavrois M, De Noronha C, Greene WC. A sensitive and specific enzyme-based assay detecting HIV-1 virion fusion in primary T lymphocytes. *Nat Biotechnol.* 2002;20(11):1151-1154.
85. O'Doherty U, Swiggard WJ, Malim MH. Human immunodeficiency virus type 1 spinoculation enhances infection through virus binding. *J Virol.* 2000;74(21):10074-10080.
86. Suzuki K, Shijuuku T, Fukamachi T, et al. Prolonged transcriptional silencing and CpG methylation induced by siRNAs targeted to the HIV-1 promoter region. *J RNAi Gene Silencing.* 2005;1(2):66-78.



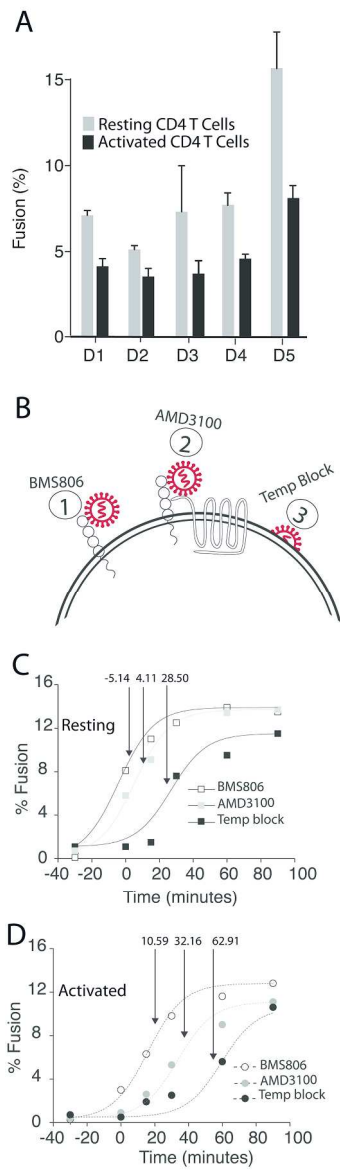
Small molecule inhibition of dynamin observes HIV inhibition profiles consistent with entry and post-entry



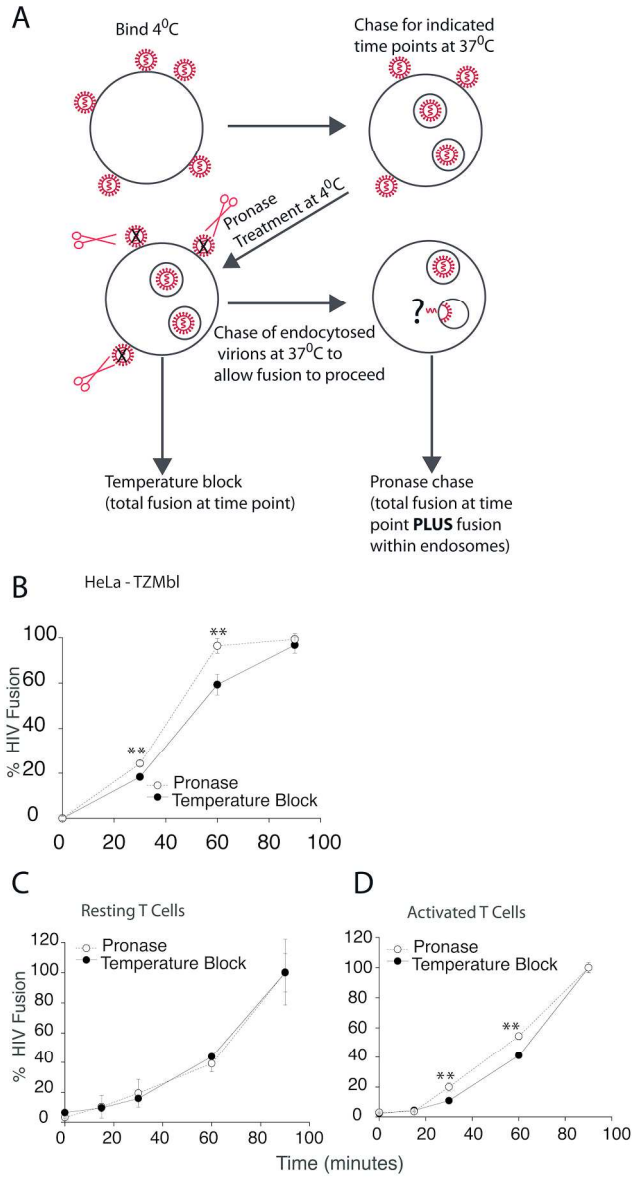
Resolution of HIV post-entry blocks through dynamin inhibition



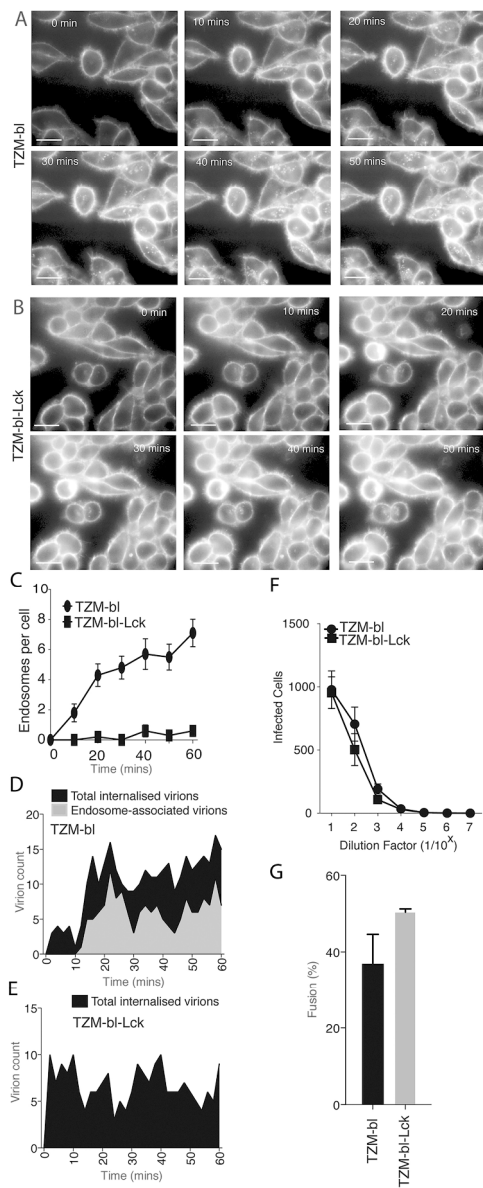
HIV endocytosis in primary resting CD4 T cells is limited and is increased through T cell activation



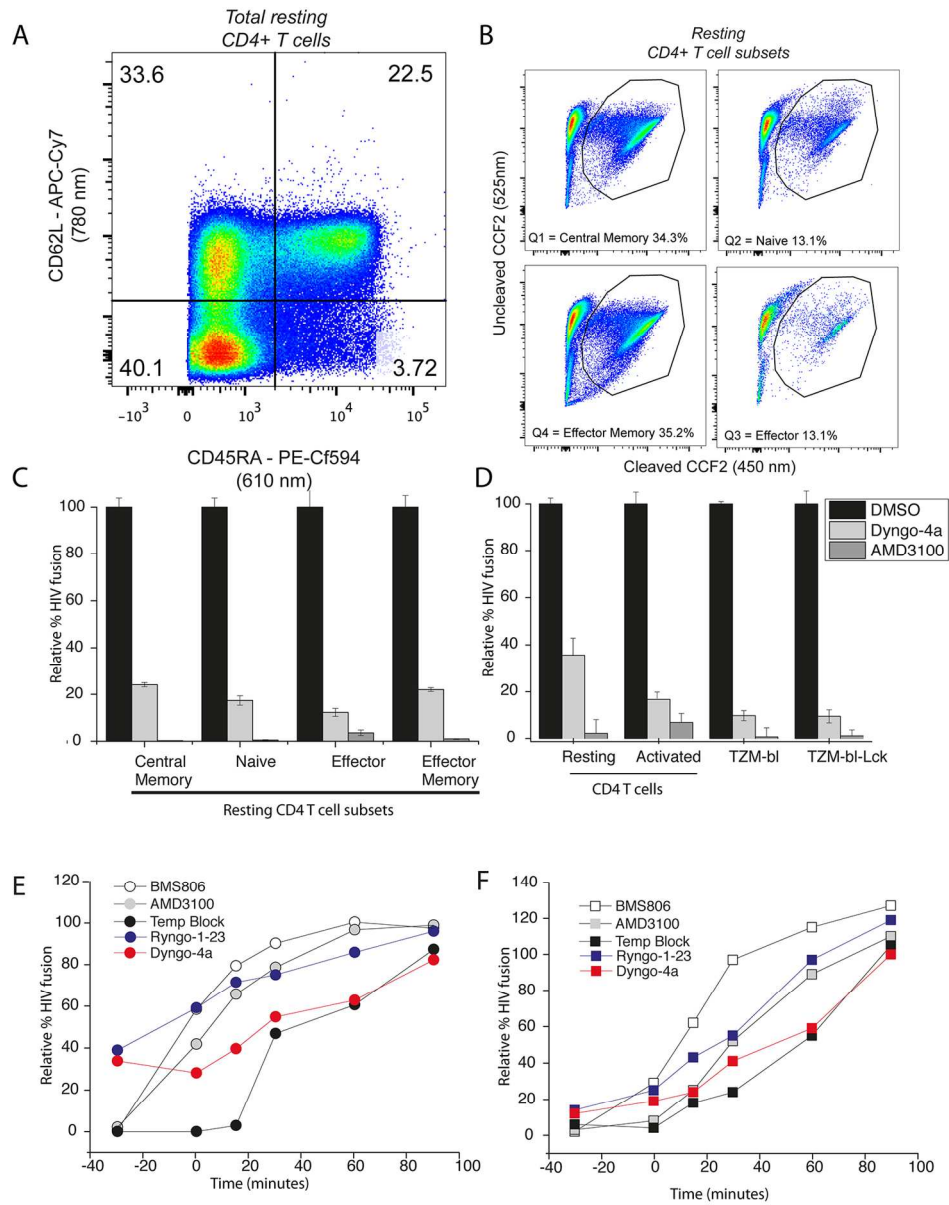
HIV fusion kinetics in resting and activated CD4 T cells



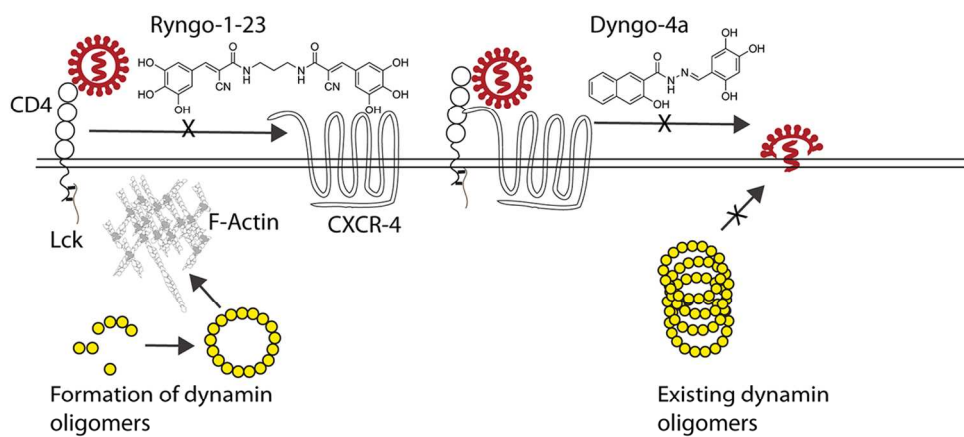
HIV is surface accessible in resting CD4 T cells throughout the duration of the fusion reaction



Role of Lck in CD4 plasma membrane tethering in HeLa cells



Dynamin inhibition blocks HIV



Proposed HIV fusion blocks mediated by ryngo-1-23 and dyngo-4a